CHAPTER–3

Activation of Small Molecules by Cyclic Alkyl Amino Silylenes (CAASis) and Germylenes (CAAGes): A Theoretical Study

Abstract: Quantum chemical calculations have been carried out on a series of skeletally modified cyclic alkyl amino silylenes (CAASis) and germylenes (CAAGes) to understand their ligand properties and reactivity towards the activation of a variety of small molecules. Installation of boron or silicon atom into the ring framework of these silylenes/germylenes led to dramatic increase in their σ–basicity while incorporation of ylidic moieties resulted in sharp reduction of their π-acidity although it did help in increasing the electron donation ability. The calculated values of energy barriers for activation of H–H, N–H, C–H and Si–H bonds by many of the cyclic silylenes considered here are found to be comparable to those with experimentally evaluated systems indicating the potential of these computationally designed molecules in small molecule activation and calls for synthetic efforts towards their isolation. Further, activations employing CAAGes are found to be more demanding than those with CAASis which may be attributed to the significantly lower Lewis basicity of the former than the latter.

[3.1] Introduction

The chemistry of silylenes and germylenes are fairly diverse both in structure and reactivity. *N*-heterocyclic silylene (NHSi) **Ia** [1] (Scheme 3.1) and germylene (NHGe) **Ib** [2] are neutral divalent species with a vacant p–orbital and a non–bonding pair of electrons. A majority of the silylenes and germylenes possess a singlet ground state which may be attributed to the increased radial extension of ns and np orbitals as we go down the group [3]. The ligating properties of NHEs (E = Si, Ge) are somewhat different from their lighter congeners as NHCs possess a higher Lewis basicity and lower Lewis acidity than NHSis/NHGes [4].

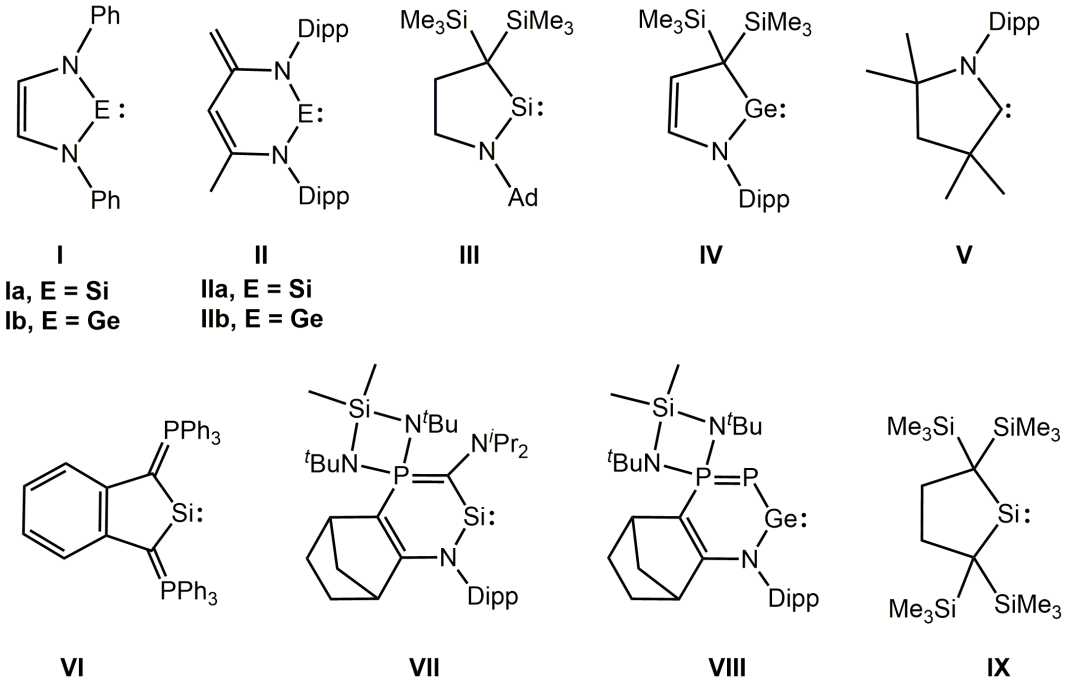

Scheme 3.1: Schematic presentation of synthetically attainable carbene, silylenes and germylenes discussed in the present study.

A steady growth was marked in the field of stable silylenes and they were found to react with main group elements, organic substrates as well as the transition metals [5]. Later, NHGes were also reported to form complexes with transition metals [6]. Driess and co-workers were successful in the isolation of zwitterionic NHSi (**IIa**) [7] and NHGe (**IIb**) [8] supported by a modified β–diketiminate ligand framework. These new types of NHSis and NHGes are found to have unique electronic features and strikingly different reactivities which enables metal–free activation of small molecules like NH_3

[9], P_4 [10], etc. Later, different independent groups came up with some more silylenes and also complexes featuring the silicon center in various oxidation states [11]. Recently, the research groups of Iwamoto [12] and Kinjo [13] independently reported the isolation of Si (**III**) and Ge (**IV**) analogs of cyclic(alkyl)(amino)carbene (CAAC, **V**) [14] where the central silicon or germanium atom is bonded to a nitrogen and a quaternary carbon atom. These cyclic(alkyl)(amino)silylenes (CAASi) and cyclic(alkyl)(amino)germylenes (CAAGe) are found to have better electron donation ability than classical NHSis and NHGes. It may be noted that the ambiphilic property of CAAC led to its vast application in stabilization of low valent transition metal complexes and main group element species [15]. CAACs were also found to be useful in the activation of various small molecules like H_2, NH_3 [16], CO [17] and bonds such as B–H, P–H and Si–H [18].

In 2011, Driess and co-workers reported an aromatic ylide-stabilised silylene (**VI**) [19] which demonstrates that replacement of the two amino groups of the NHSi ring with more electron rich and less electronegative ylide moiety leads to an enhancement of the σ-basicity of the "ene" center. Kato and co-workers reported the isolation of cyclic amino(ylide)silylene (**VII**) [20] and amino(phosphanylidene-σ^4-phosphorane) germylene (**VIII**) [21] both of which have higher reactivity toward transition metals compared to the classical NHSis and NHGes respectively. Similarly, Kira and co-workers could successfully isolate a cyclic dialkysilylene (**IX**) [22] which can activate Si–Cl and Si–H bonds of various silanes [23]. Very recently, Iwamoto and co-workers found that CAASi could be used as a dehydrogenation reagent [24]. However, compared to the large number of studies being carried out on CAACs, to the best of our knowledge, there exists no systematic and comprehensive study–either experimental or computational, on CAASis and CAAGes. Herein, we present our results of computational studies on the electronic and ligand properties of skeletally substituted CAASis and CAAGes and based on their ligand properties, some of these molecules are probed towards activation of small molecules (Scheme 3.2). Our choice of the carbonyl group and phosphorus ylide as substituents was inspired by earlier reports of their use towards enhancing the π-acidity and σ-basicity respectively [19, 25].

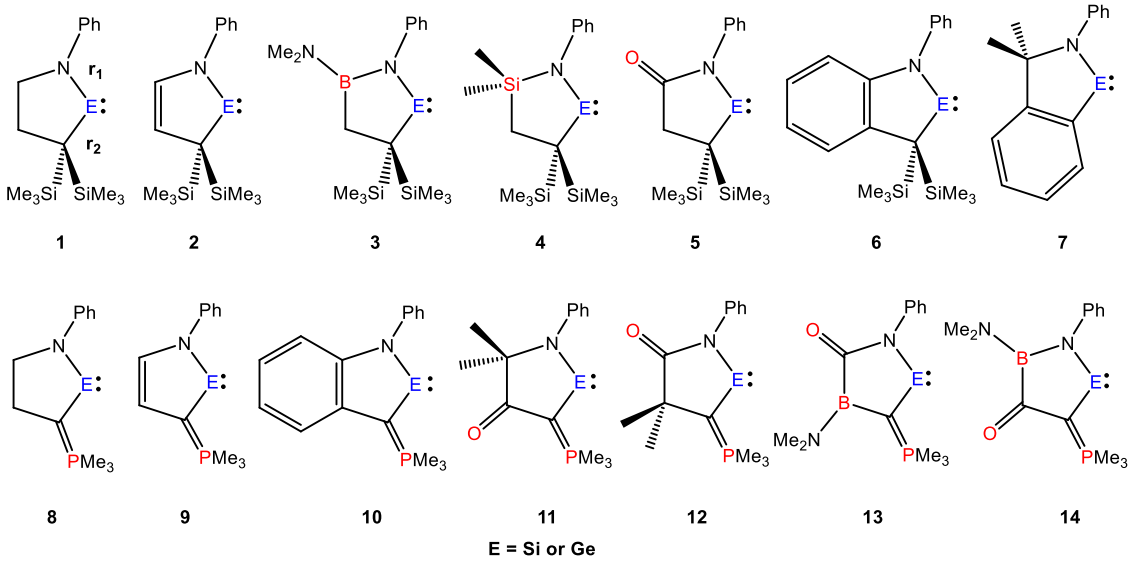

Scheme 3.2: Schematic representation of the range of silylenes and germylenes considered in the present study [26]. [r_1 and r_2 are the distances between the ene center (E) and α-nitrogen atom (E–N) and α-carbon atom (E–C) respectively].

[3.2] Computational Details

Density functional theory calculations were carried out to optimize all the molecules without any symmetry constraints using the meta-GGA M06 exchange correlational functional in conjunction with def2-TZVP basis set for all the atoms [27a, 28]. Our Choice of the meta-GGA M06 exchange-correlation functional in conjunction with the def2-TZVP basis set is inspired from the fact that this combination of functional and basis set could reproduce the geometrical parameters of the experimentally isolated CAASi (**1Si**) and CAAGe (**2Ge**) (Table 3.1). In addition, M06 functional is widely used to study different molecular properties of main group as well as transition metal complexes [27]. Frequency calculations were performed at the same level of theory to characterize the nature of the stationary points. The ground states are characterized by the presence of real vibrational frequencies while the transition states are characterized by the presence of only one imaginary frequency. The characterization of the transition states were further probed by performing intrinsic reaction coordinate (IRC) analysis which connects the correct pathways to both the products and reactants. For calculating the activation energy barriers, the relative energies are evaluated with respect to the sum of the energies of the separated reactants. Natural bonding analysis was performed with the natural bond orbital (NBO) [29] partitioning scheme as implemented in the Gaussian 09 suite of programs [30]. Solvent (Tolune) and dispersion effects were incorporated for all the molecules by using the polarizable continuum model (PCM) [31] and the D3 version of

Grimme's dispersion correction [32] coupled with the D3 damping function using the keyword "Empirical Dispersion=GD3" as implemented in Gaussian 09 quantum package. The energetics were evaluated for all the calculations in Gibbs free energies at 298K and 1atm pressure unless otherwise specified.

[3.3] Results and Discussion

The central ring of **1**, **3**–**5**, **8** and **12**–**14** (for both CAASis and CAAGes) are found to have distorted structures while the rest acquires perfectly planar geometries (Figure 3.1). The important geometrical parameters and Wiberg Bond Index (WBI) values of **1**–**14** in their optimized singlet states are collected in Table 3.1. It is evident from Table 3.1 that the calculated geometrical parameters of the parent CAASi (**1Si**) and CAAGe (**2Ge**) are in excellent agreement with the experimentally observed values. Replacement of the alkyl group at position α to the "ene" center in **1**, **2** and **6** by an ylide moiety [26] resulting in structures **8**, **9** and **10** dramatically increases and decreases the r_1 and r_2 (Scheme 3.2) bond lengths respectively (Table 3.1). This indicates an increase in electronic delocalization from the ylidic lone pair to the formally vacant p–orbital at Si or Ge center than that between the lone pair at nitrogen (LP_N) and "ene" center. In fact, this interaction is also evident from their corresponding WBI values (Table 3.1). We also obtained an appreciable change in both the r_1 and r_2 bond lengths as a result of systematic installation of carbonyl group at different positions in the backbone of the ring scaffold of **8** (i.e. in **11** and **12**). The r_1 and r_2 bonds of **11** are found to decrease and increase respectively than that in **8** while in case of **12** the r_1 and r_2 bonds are longer and shorter respectively than that in **8** (Table 3.1). Such variations in bond lengths may be attributed to the delocalization of LP_N to the empty anti-bonding orbital of the carbonyl group (π^*_{CO}).

There is precedence in the literature for the evaluation of thermodynamic stability of divalent group 14 bases in terms of calculated singlet-triplet energy separation ($\Delta E_{S\text{-}T}$) values [33]. In principle, a greater singlet state stability is expected for a divalent "ene" molecule with a large $\Delta E_{S\text{-}T}$ value. However, NBO analysis suggest that the spin is not localized at the "ene" center for all the molecules indicating the presence of biradical character in the triplet states of some silylenes/germylenes Table 3.2. Accordingly, the $\Delta E_{S\text{-}T}$ values of these molecules cannot be compared with those having diradical character (i.e., the spin is mostly localized at the ene center. The bar diagrams in

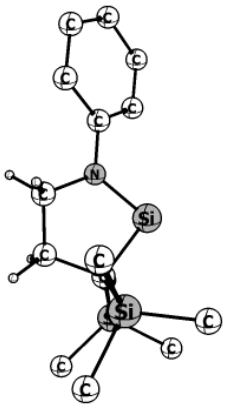

1Si

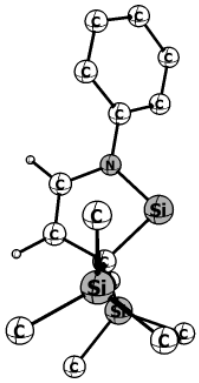

2Si

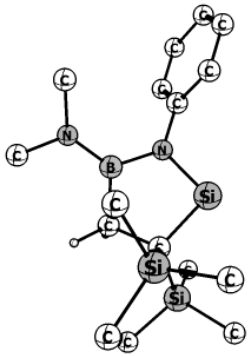

3Si

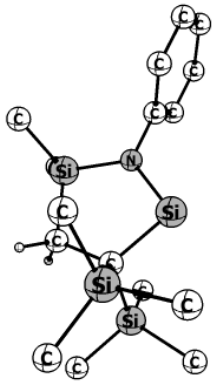

4Si

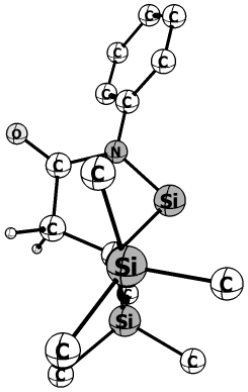

5Si

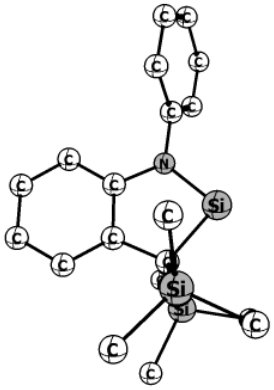

6Si

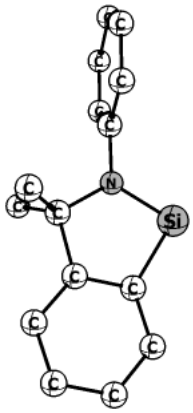

7Si

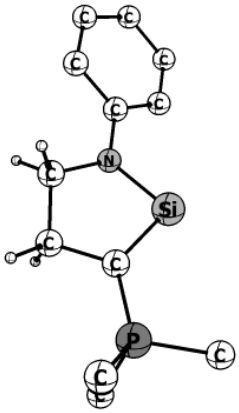

8Si

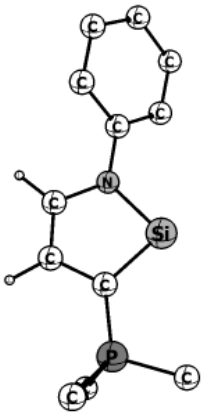

9Si

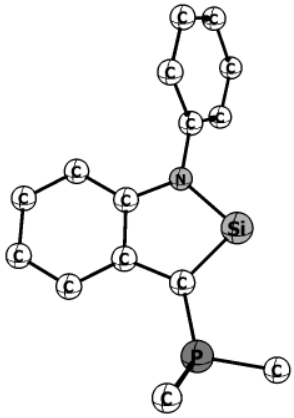

10Si

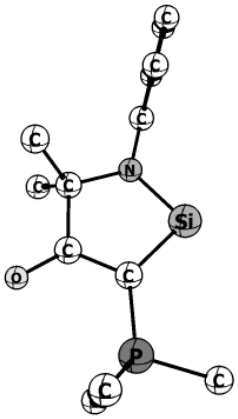

11Si

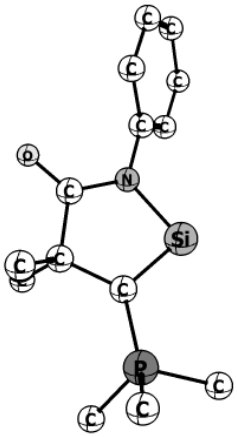

12Si

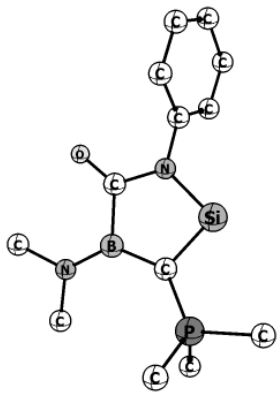

13Si

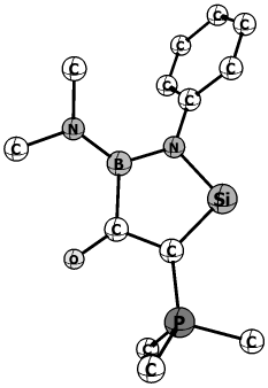

14Si

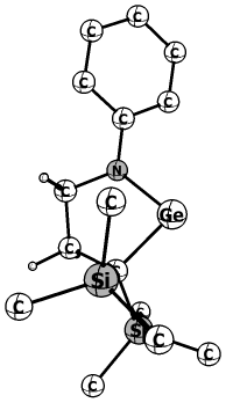

1Ge

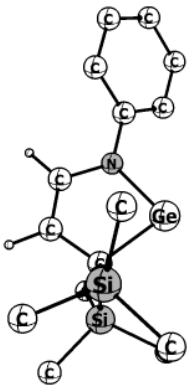

2Ge

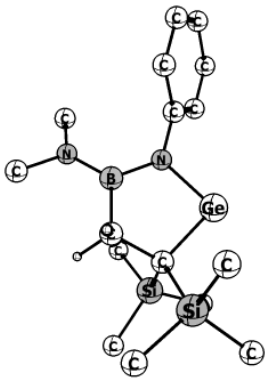

3Ge

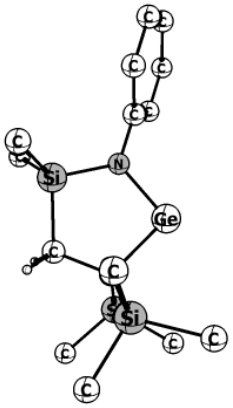

4Ge

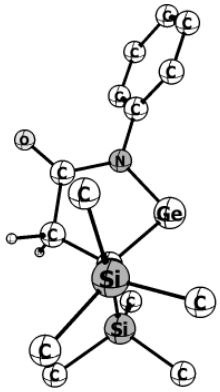

5Ge

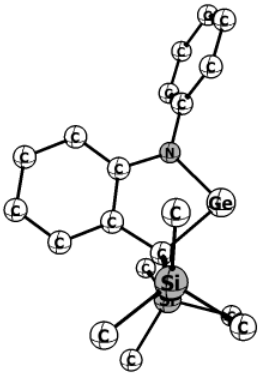

6Ge

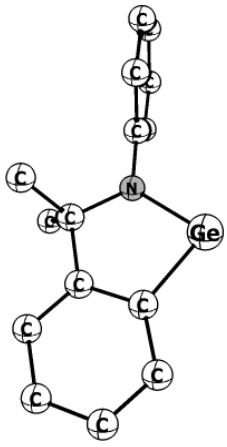

7Ge

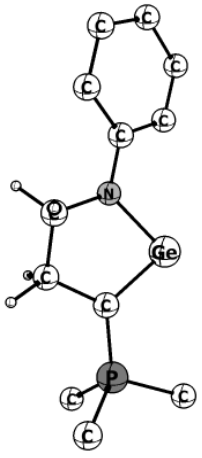

8Ge

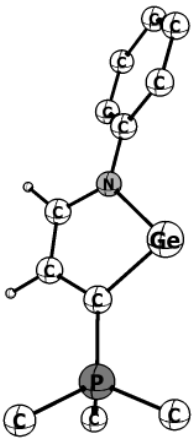

9Ge

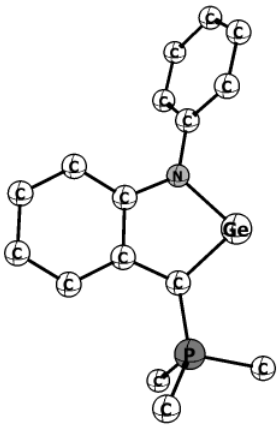

10Ge

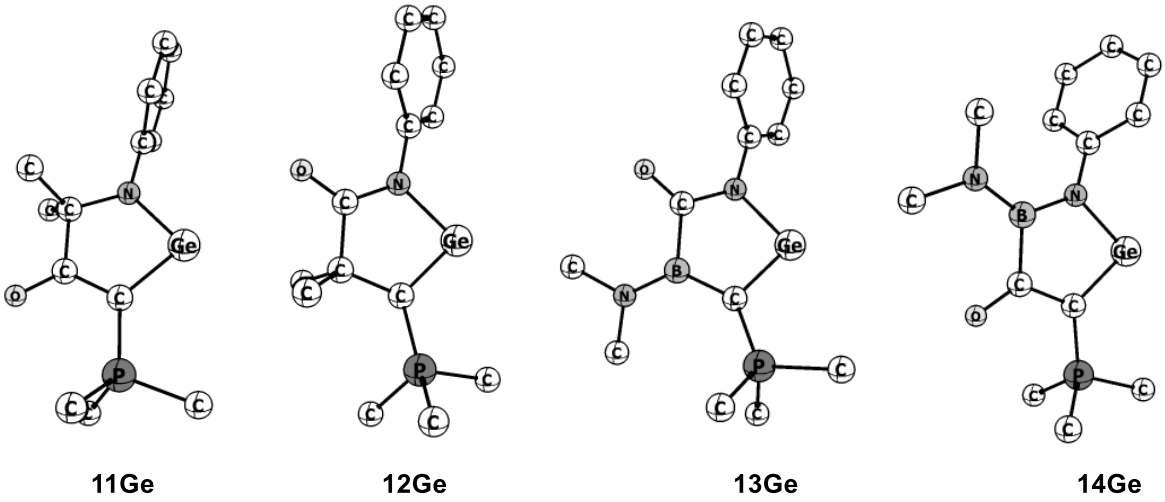

Figure 3.1: Singlet state optimized geometries of **1-14** at M06-D3/def2-TZVP (Toluene) level of theory. The hydrogen atoms of the phenyl and methyl groups are omitted for the sake of clarity.

Table 3.1: Calculated (M06-D3/def2-TZVP (Toluene)) X–E bond lengths (r_1/r_2 in Å), Wiberg Bond Index (WBI) values and ∠X–E–X bond angles (in degrees) of the singlet state geometry of **1–14** (X = N or C and E =Si or Ge). The experimental values are given within parenthesis.

Molecule	E–X(r_1/r_2)	WBI(r_1/r_2)	∠X–E–X	Molecule	E–X(r_1/r_2)	WBI(r_1/r_2)	∠X–E–X
1Si	1.742/1.900 (*1.714/1.914*)	0.711/0.676	91.5 (*92.6*)	**1Ge**	1.869/2.012	0.704/0.680	87.7
2Si	1.766/1.901	0.703/0.704	89.0	**2Ge**	1.893/2.003 (*1.859/1.998*)	0.680/0.706	85.6 (*86.5*)
3Si	1.751/1.895	0.645/0.674	93.5	**3Ge**	1.876/2.003	0.642/0.685	89.9
4Si	1.728/1.910	0.689/0.675	97.0	**4Ge**	1.856/2.024	0.688/0.688	93.7
5Si	1.763/1.890	0.622/0.678	91.1	**5Ge**	1.888/1.997	0.613/0.688	87.6
6Si	1.748/1.911	0.697/0.677	89.6	**6Ge**	1.871/2.014	0.683/0.683	86.1
7Si	1.725/1.885	0.792/0.754	88.1	**7Ge**	1.844/1.980	0.764/0.743	84.7
8Si	1.784/1.796	0.650/1.024	89.8	**8Ge**	1.926/1.918	0.652/0.998	83.6
9Si	1.798/1.826	0.696/1.005	87.0	**9Ge**	1.926/1.918	0.652/0.998	83.6
10Si	1.782/1.823	0.676/0.971	88.1	**10Ge**	1.907/1.915	0.635/0.968	84.5
11Si	1.735/1.832	0.744/0.847	89.5	**11Ge**	1.854/1.926	0.722/0.845	86.0
12Si	1.801/1.794	0.581/1.040	89.4	**12Ge**	1.931/1.885	0.542/1.049	85.8
13Si	1.781/1.819	0.599/0.901	94.2	**13Ge**	1.914/1.912	0.561/0.909	90.5
14Si	1.778/1.819	0.616/ 0.883	92.4	**14Ge**	1.908/1.911	0.579/0.891	88.8

Figure 3.2 represents the variation of ΔE_{S-T} values for all the molecules. Irrespective of the nature of the triplet states, the ΔE_{S-T} values of the skeletally substituted CAASis (46.7-62.4 kcal mol^{-1}) are either comparable or higher than that of the experimentally isolated **1Si** (50.8 kcal mol^{-1}). In contrast, compared to the synthetically achievable CAAGe (**2Ge**) that has a ΔE_{S-T} value of 39.0 kcal mol^{-1}, all other germylenes considered in this study has significantly higher values (42.9-56.5 kcal mol^{-1}).

Table 3.2: Calculated (M06-D3/def2-TZVP (Toluene)) Mulliken spin density at the central atom (E =Si/Ge), α-nitrogen (N_α) and carbon (C_α) atom (with respect to the central atom) and occupancies of the formally vacant valence p-orbital (Occ) at the central atom (Si/Ge) for **1Si-14Si** and **1Ge-14Ge**.

Molecule	Si	N_α	C_α	Occ	Molecule	Ge	N_α	C_α	Occ
1Si	1.446	0.125	0.281	0.256	**1Ge**	0.917	0.429	0.148	0.291
2Si	1.098	0.225	0.202	0.301	**2Ge**	1.029	0.284	0.145	0.310
3Si	1.477	0.083	0.319	0.388	**3Ge**	1.271	0.096	0.498	0.265
4Si	1.471	0.066	0.267	0.212	**4Ge**	1.248	0.036	0.449	0.286
5Si	1.558	0.088	0.215	0.182	**5Ge**	1.292	0.064	0.554	0.176
6Si	1.229	0.206	0.240	0.288	**6Ge**	1.024	0.329	0.176	0.288
7Si	1.566	0.105	0.019	0.240	**7Ge**	0.834	0.502	-0.105	0.241
8Si	0.847	0.078	0.718	0.360	**8Ge**	0.884	0.078	0.715	0.353
9Si	0.967	0.137	0.184	0.531	**9Ge**	0.951	0.167	0.205	0.530
10Si	1.045	0.115	0.273	0.426	**10Ge**	0.996	0.146	0.265	0.442
11Si	1.600	0.095	0.096	0.294	**11Ge**	0.828	0.506	0.036	0.298
12Si	0.890	0.052	0.656	0.346	**12Ge**	0.904	0.057	0.671	0.348
13Si	1.496	0.026	0.152	0.276	**13Ge**	0.924	0.103	0.667	0.278
14Si	1.407	0.032	0.103	0.262	**14Ge**	0.885	0.355	0.159	0.262

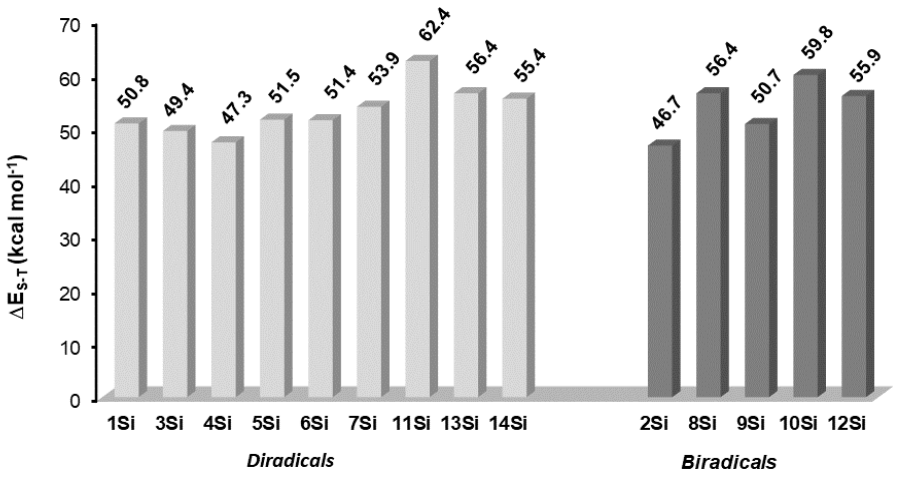

(a)

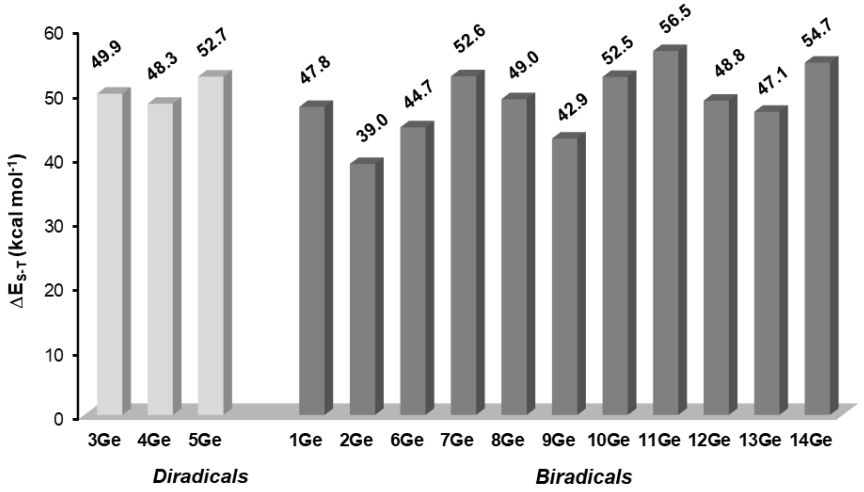

(b)

Figure 3.2: Bar diagrams representing the ΔE_{S-T} gaps of (a) cyclic alkyl amino silylenes (CAASis) and (b) cyclic alkyl amino germylenes (CAAGes) considered in the present study.

The reactivity and ligand properties of these CAASis and CAAGes can be well understood by studying the nature and energies of their key frontier molecular orbitals (Figure 3.3). In general, higher is the energy of the donor orbital, higher is its donor ability while lower is the energy of the acceptor orbital, higher is its acceptance ability. Further, for the sake of comparison, Figure 3.3 also includes the energies of the σ-symmetric donor (E_σ) and π-symmetric acceptor (E_π*) orbital of NHSi/NHGe (**I**). It is obvious from Figure 3.3 that all of the CAASis/CAAGes (**1-14**) exhibits significantly enhanced electron donation as well as accepting ability (except **8**-**12**) compared to **I**

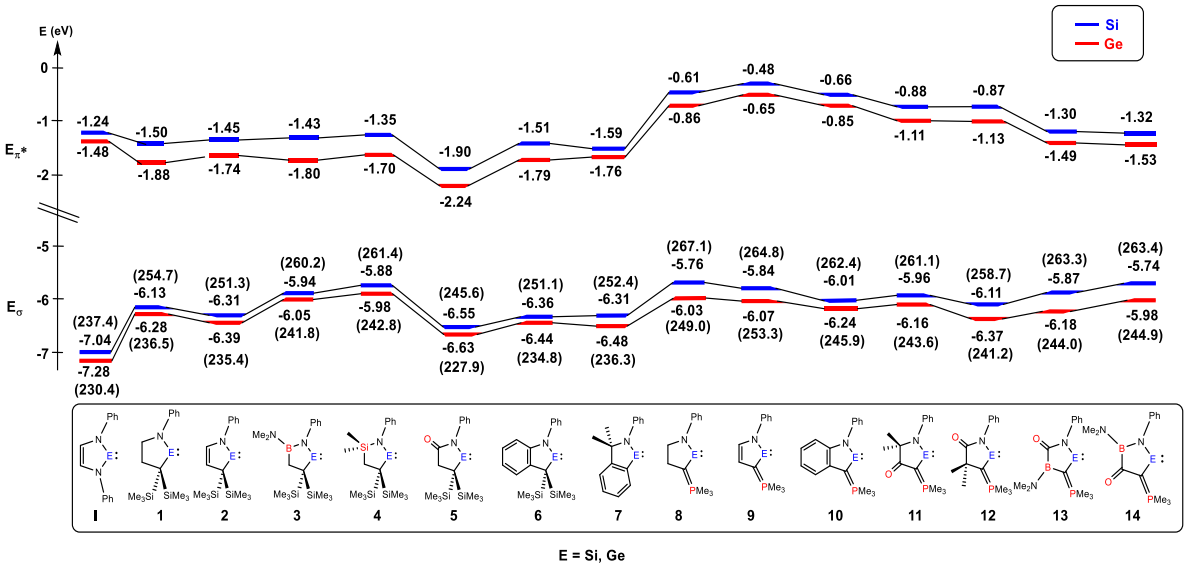

Figure 3.3: Calculated (M06-D3/def2-TZVP (Toluene)) energies (in eV) of the occupied σ–symmetric donor (E_{σ}) and unoccupied π–symmetric acceptor (E_{π}*) molecular orbitals concentrated at the Si/Ge atom of the silylenes and germylenes **1**–**14** and **I**. The proton affinity (PA in kcal mol^{-1}) values are given within parenthesis.

which may be attributed to the replacement of one of the amino nitrogen atoms of the silylene or germylene framework of **I** by a less electronegative alkyl group [12, 13]. Further, it is evident from Figure 3.3 that compound **2** with an unsaturated backbone possess somewhat lower σ–donation (low E_{σ}) and π–acceptance (low E_{π}*) abilities than **1** with a saturated backbone. The introduction of boron and silicon centre next to the α–amino group of **1** (i.e., in **3** and **4**) results in an increase and decrease in σ–donation (**1**< **3** < **4**) and π–acceptance ability (**1**> **3** > **4**), respectively. Interestingly, a significant reduction and enhancement of σ–donation and π-acidity respectively is observed as a result of incorporation of electron withdrawing carbonyl group (in **5**) in the ring framework of **1**. On the other hand, introduction of benzene moiety in the backbone of the ring framework (in **6**) and at position α with respect to the Si/Ge center (in **7**) of the parent molecule marginally decreases the σ-donation ability. The π-acceptance ability of **6Si** and **7Si** are comparable to that of **1Si** while that of **6Ge** and **7Ge** are slightly lower than that of **1Ge**. Replacement of the two silyl groups attached to the α–carbon atom with respect to the "ene" center in **1**, **2** and **6** by the more electron releasing ylide group (in **8**, **9** and **10**) dramatically increases and decreases the σ–donation and π–acceptance ability respectively. Incorporation of the π–electron withdrawing carbonyl group next to the ylide/α–amino moiety of **8** (i.e., in **11** and **12**) results in decrease and increase in σ–

basicity and π–acidity respectively. However, the increase in π–acceptance ability is more rewarding in case of molecules **13** and **14** as a result of installation of both carbonyl group and boron atom, respectively, in the backbone of the ring scaffold of **8**. Among all the silylenes and germylenes, **5** are found to have the highest and lowest π–acidity and σ–basicity respectively.

The σ–donation ability of these silylenes and germylenes can be gauged from an evaluation of their respective proton affinity (PA) values. In principle, molecules with higher σ–donation ability also have higher PA values. The calculated PA values for the ylide anchored silylenes and germylenes are found to be higher than the non-ylidic ones. For example, replacement of the alkyl group adjacent to the Si/Ge center in **1**, **2** and **6** by ylide moieties (in **8**, **9** and **10**) leads to enhancement of the PA values (Figure 3.3) which is in agreement with their respective E_σ values. Indeed, we obtain a nice (R^2 = 0.94) and reasonable (R^2 = 0.67) correlation between E_σ and PA values for all the silylenes and germylenes respectively (Figure 3.4).

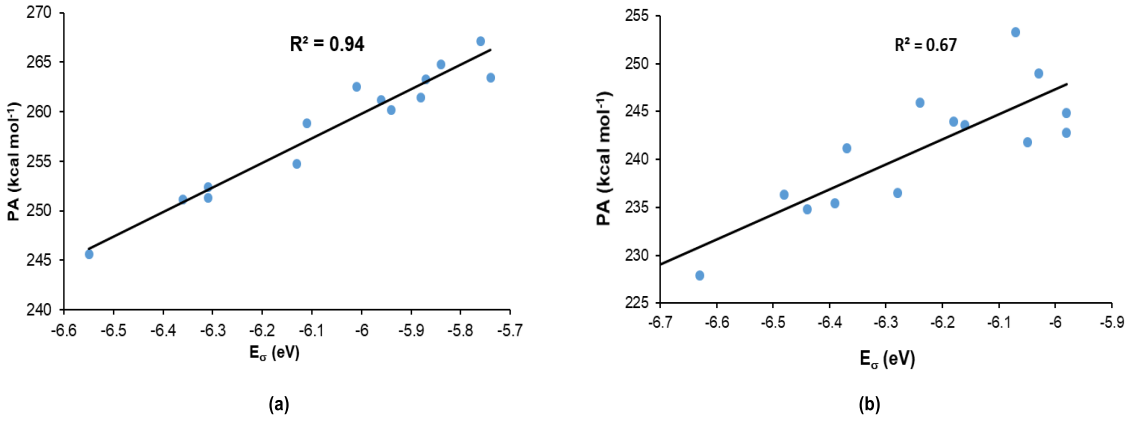

Figure 3.4: Correlation plots between the E_σ (eV) and PA (kcal mol^{-1}) for (a) silylenes (**1Si**–**14Si)** and (b) germylenes (**1Ge**–**14Ge**).

From the above discussions, it can be envisaged that since many of the computationally designed CAASis and CAAGes possess significant electron donation and acceptance abilities as that of the synthetically isolable **1Si** and **2Ge**, hence they may be considered as potential candidates for activation of a variety of small molecules. In the present study, we have considered activation of H_2, NH_3, CH_3Ph and Et_3SiH by considering compounds **1-5**, **8**, **9** and **14** as representative CAASis/CAAGes. To make the study more meaningful or relevant to synthetic chemists, wherever possible, the

energetics of the bond activations was compared with known silylene/germylene systems.

[3.3.1] Activation of Dihydrogen

Even though dihydrogen is a highly inert molecule, it is extensively used in various biological [34] as well as in chemical processes [35]. For example, reactions like hydroformylation, hydrogenation and production of ammonia involve the splitting of an enthalpically strong H–H bond as a key step. Earlier, this was achieved by using transition metal complexes that are not only expensive but can also often be less efficient and toxic [36]. To circumvent the disadvantages associated with transition metals, efforts were made to design environmentally benign main group systems. In 2005, Power and co-workers elegantly developed a digermyne complex that can readily split H_2 under ambient reaction conditions [37]. Thereafter, several main group element based compounds were reported which can activate the H–H bond under mild reaction conditions [38]. This has inspired us to undertake a mechanistic study to probe the potential of the skeletally substituted CAASis/CAAGes towards the activation of dihydrogen as most of them exhibit significantly enhanced ligand properties (**1-5**, **8**, **9** and **14**) compared to their synthetically accessible analogs.

The mechanism involved in the activation of dihydrogen by CAASi or CAAGe can be thought of as similar to that for activation of dihydrogen by CAAC [16, 39]. In other words, the lone pair at the ene center of CAASi or CAAGe interacts with the H–H antibonding orbital, thereby generating a pseudo hydridic hydrogen (H_{hy}) atom. Thereafter, the migration of the H_{hy} atom from the activated H–H bond to the vacant p_π orbital centered at the Si/Ge center yields the H–H splitting product. The overall process proceed via a transition state (TS) exhibiting a significantly elongated and polarized H–H bond. In this context, in a ground breaking study, Ess and co-workers showed that there is a significant difference between the transition state geometries involved in the activation of dihydrogen by carbenes and silylens/germylenes [38i, 39b]. The differences in the TS geometries basically occurs due to the different trajectories followed by H_2 while approaching the main group compounds during the activation process.

The reaction profile and the optimized geometries of the TSs obtained for the activation of dihydrogen by **1Si** and **1Ge** are given in Figure 3.5 as representative cases. The important calculated geometrical and electronic parameters for all the TSs are given

in Table 3.3 and Figure 3.6. It can be ascertained from Figure 3.5 and Figure 3.6 that all the TSs exhibit significantly elongated and polarized H–H bond (Table 3.3) with the H_{hy} atom remains distant from the Si/Ge center (1.764-1.825 Å). The polarization of the H–H bond as well as the *in situ* generation of H_{hy} in the TSs is corroborated from an analysis of the NBO based natural charges having values of -0.048 to -0.282 and 0.0 to 0.121 for the H_{hy} and positively polarized hydrogen atom respectively for activation by CAASis (Table 3.3). The same is true for activation by CAAGes. A comparison of the

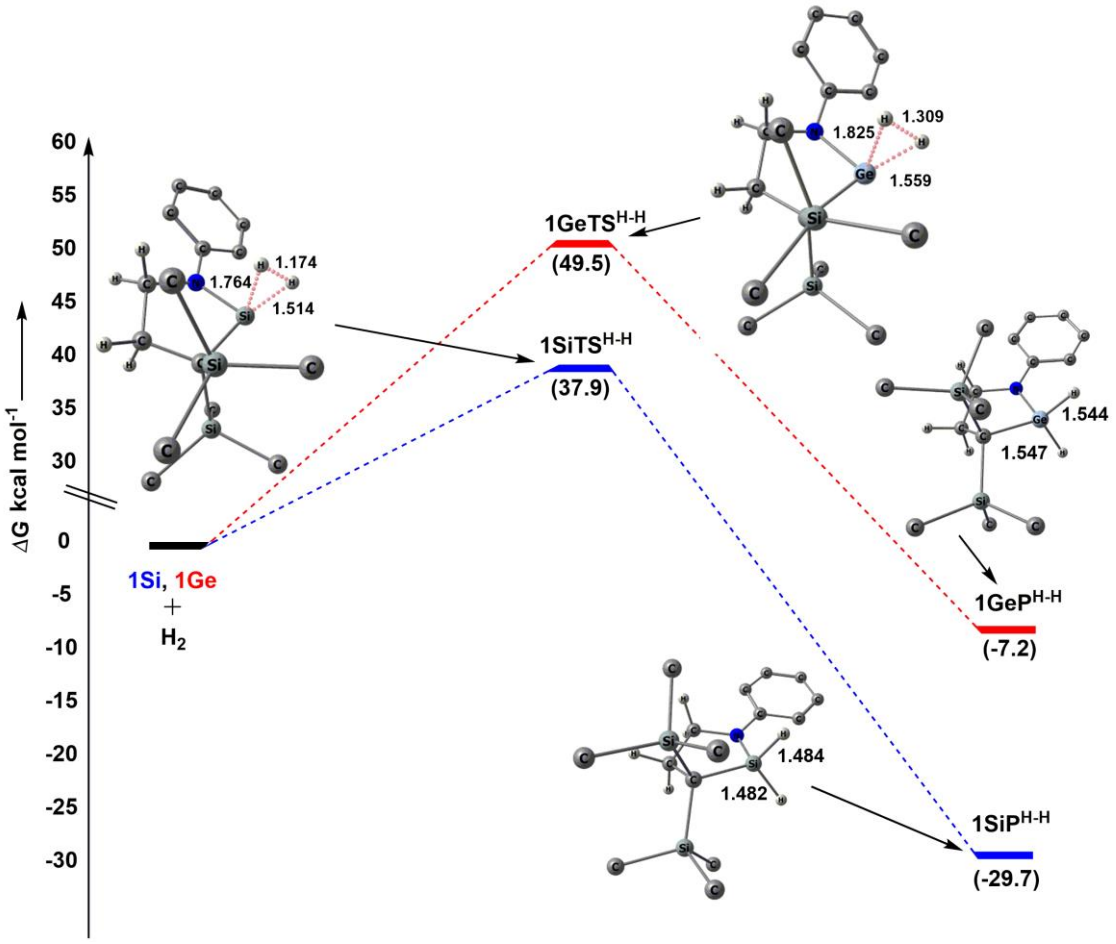

Figure 3.5: Reaction profile diagram for the activation of dihydrogen by **1Si** and **1Ge** at M06-D3/def2-TZVP (Toluene) level of theory. The hydrogen atoms of the methyl and phenyl groups are omitted for the sake of clarity.

geometrical parameters for the TSs (Table 3.3) with the respective ground state geometries of corresponding CAASis/CAAGes (Table 3.1) show that there are appreciable changes in their calculated E–X (E = Si, Ge and X = C, N) bond lengths and also all of them exhibits wider ∠C-E-N bond angles. The activation process is accompanied by a marginal to significant increase in occupancy of the formally vacant

3p orbital at the central Si atom compared to that of the free CAASis (Table 3.2 and Table 3.3) which is attributed to the interaction of the H_{hy} atom with the vacant 3p orbital. For example, the occupancy significantly increases from 0.256 in in **1Si** to 0.791 in **1SiTS^{H-H}** while the same increases only marginally from 0.388 in **3Si** to 0.484 in **3SiTS^{H-H}**.

Table 3.3: Calculated (M06-D3/def2-TZVP (Toluene)) important geometrical parameters and natural charges at pseudo hydridic ($q_{H_{hy}}$) and positively polarized hydrogen atom (q_H) and occupancies of the formally vacant p-orbital ($Occ_{Si/Ge}$) of the transition states involved in the activation of hydrogen by CAASis (**1Si-5Si**, **8Si-9Si** and **14Si**) and CAAGes (**1Ge-5Ge**, **8Ge-9Ge** and **14Ge**). Bond lengths (E – X, E = Si, Ge and X = N, C), bond angles (∠C-E-N) are given in Å and in degree (°) respectively.

Molecules	H_{hy} – H	E – H	E – H_{hy}	E - X	∠C-E-N	$Occ_{Si/Ge}$	$q_{H_{hy}}$	q_H
1SiTS^{H-H}	1.174	1.514	1.764	1.746/1.879	96.8	0.791	-0.080	0.121
2SiTS^{H-H}	1.184	1.512	1.732	1.765/1.883	95.0	0.596	-0.055	0.029
3SiTS^{H-H}	1.151	1.520	1.756	1.751/1.880	98.9	0.484	-0.064	0.014
4SiTS^{H-H}	1.145	1.521	1.747	1.744/1.894	103.3	0.928	-0.062	0.012
5SiTS^{H-H}	1.180	1.510	1.732	1.770/1.873	95.8	0.671	-0.048	0.034
8SiTS^{H-H}	1.238	1.507	1.871	1.757/1.783	95.5	0.579	-0.171	-0.001
9SiTS^{H-H}	1.303	1.502	2.029	1.750/1.799	94.1	0.783	-0.282	-0.028
14SiTS^{H-H}	1.191	1.510	1.845	1.750/1.808	96.6	0.665	-0.133	-0.001
1GeTS^{H-H}	1.309	1.559	1.825	1.874/1.977	93.3	0.814	-0.108	0.037
2GeTS^{H-H}	1.316	1.557	1.804	1.885/1.975	91.6	0.603	-0.089	0.041
3GeTS^{H-H}	1.282	1.563	1.841	1.874/1.978	95.7	0.739	-0.177	0.028
4GeTS^{H-H}	1.287	1.565	1.819	1.866/1.984	98.7	0.535	-0.101	0.026
5GeTS^{H-H}	1.310	1.556	1.798	1.889/1.968	92.0	0.550	-0.079	0.044
8GeTS^{H-H}	1.351	1.548	1.898	1.877/1.887	92.3	0.625	-0.173	0.022
9GeTS^{H-H}	1.413	1.541	2.042	1.866/1.888	91.0	0.759	-0.294	-0.001
14GeTS^{H-H}	1.320	1.550	1.902	1.868/1.891	93.2	0.697	-0.171	0.017

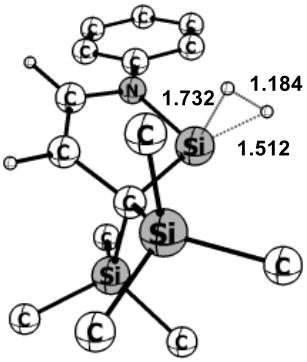

2SiTS^{H-H}

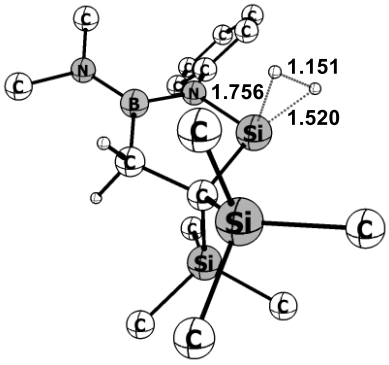

3SiTS^{H-H}

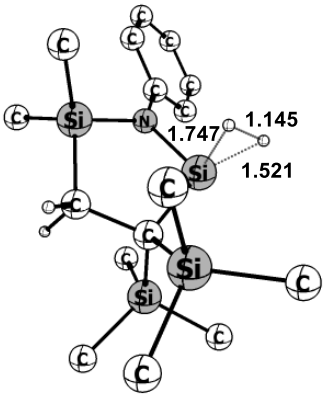

4SiTS^{H-H}

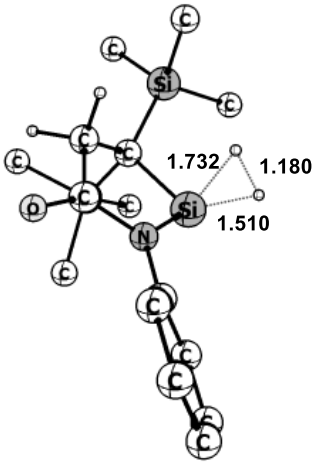

5SiTS^{H-H}

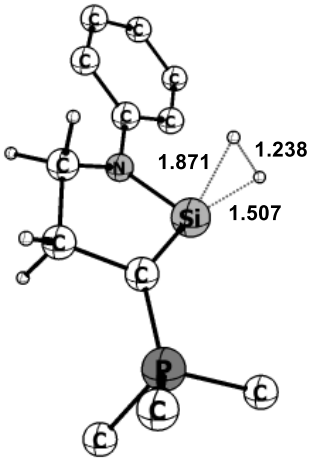

8SiTS^{H-H}

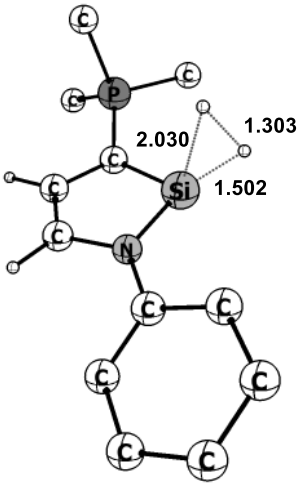

9SiTS^{H-H}

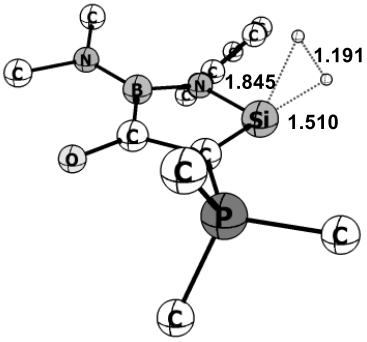

14SiTS^{H-H}

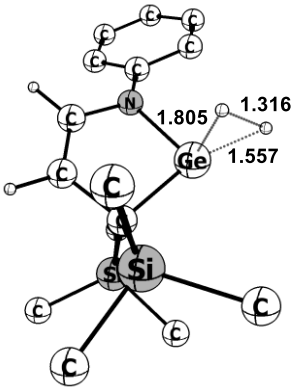

2GeTS^{H-H}

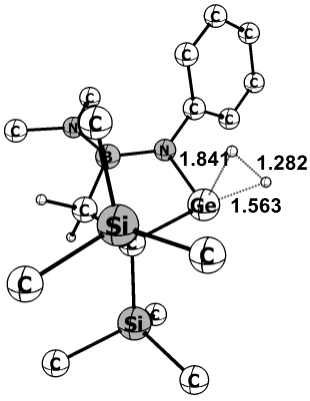

3GeTS^{H-H}

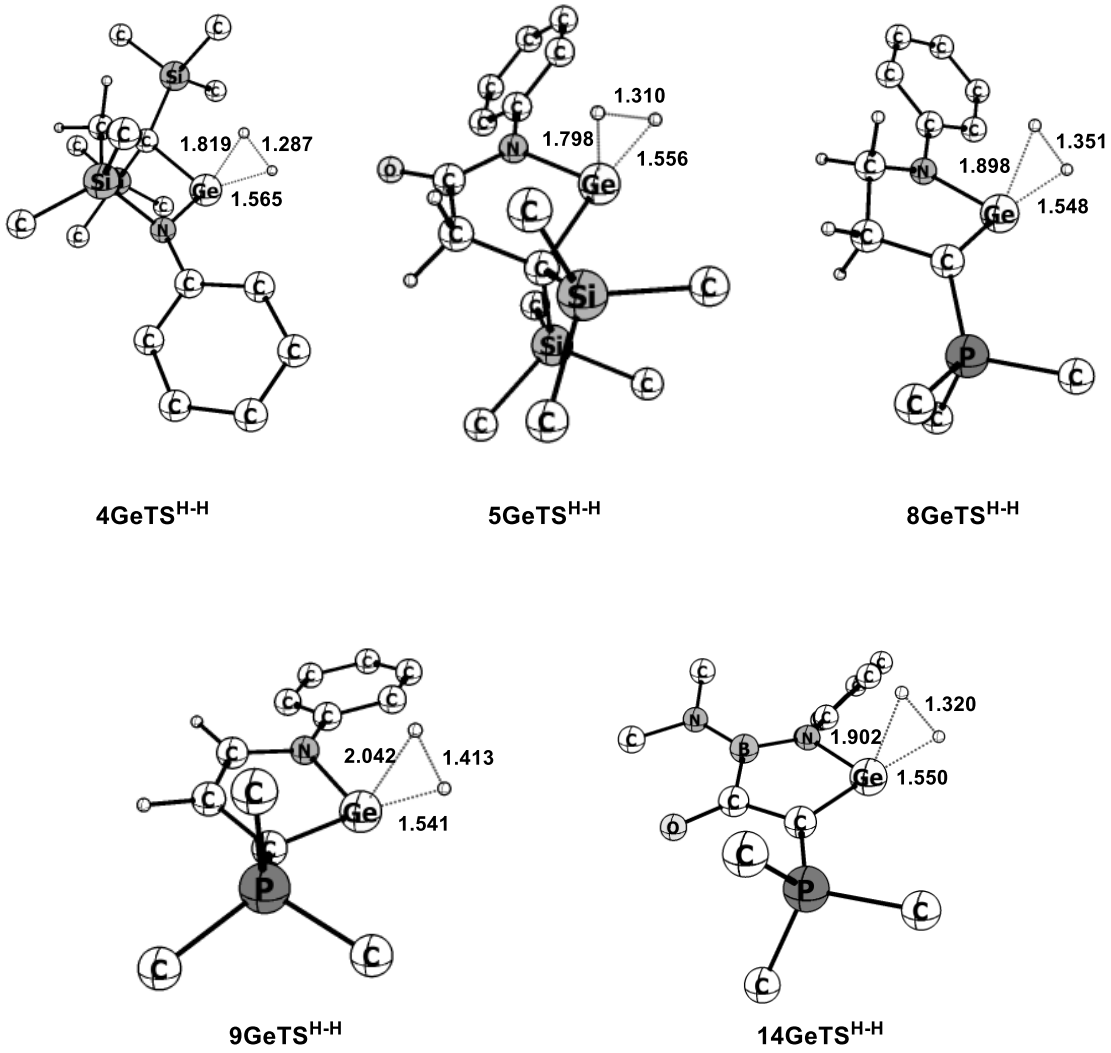

Figure 3.6: Optimized geometries for the transition states involved in the activation of dihydrogen by CAASis (**2Si-5Si**, **8Si-9Si** and **14Si**) and CAAGes (**2Ge-5Ge**, **8Ge-9Ge** and **14Ge**) at M06-D3/def2-TZVP (Toluene) level of theory. The hydrogen atoms of the phenyl and methyl groups are omitted for clarity.

The calculated reaction free energies (-11.9 to -31.0 kcal mol^{-1}) indicate feasibility of the H–H cleavage reaction by these CAASis. The computed activation free energy barriers ($\Delta G°_{TS^{H-H}}{}^{‡}$) are found to lie within 37.0 – 54.2 kcal mol^{-1} and this perhaps explain the inertness of **1Si** towards dihydrogen even at 150°C [12]. Further, the barrier heights computed for **3Si-5Si** are found to be comparable to that of the experimentally isolated **1Si** (Table 3.4) as well as that obtained for Driess's zwitterionic *β*-diketiminate stabilized *N*-heterocyclic silylene (**IIa**, Scheme 3.1) by Sicilia and co-workers [40]. However, despite having high electron donation ability, the ylide

decorated CAASis **8Si** and **9Si** (Figure 3.3) computes significantly higher $\Delta G°_{TS^{H-H}}{}^{‡}$ values (49.1-54.2 kcal mol^{-1}, Table 3.4) which may be attributed to their low electrophilicity.

Table 3.4: Calculated (M06-D3/def2-TZVP (Toluene)) activation energy barrier ($\Delta G°_{TS^{H-H}}{}^{‡}$, kcal mol^{-1}) and reaction free energies ($\Delta G°_{Total^{H-H}}$, kcal mol^{-1}) for the activation of hydrogen by CAASis (**1Si-5Si**, **8Si**, **9Si** and **14Si**) and CAAGes (**1Ge-5Ge**, **8Ge**, **9Ge** and **14Ge**).

Molecules	$\Delta G°_{TS^{H-H}}{}^{‡}$	$\Delta G°_{Total^{H-H}}$	Molecules	$\Delta G°_{TS^{H-H}}{}^{‡}$	$\Delta G°_{Total^{H-H}}$
1Si	37.9	-29.7	**1Ge**	49.5	-7.2
2Si	43.8	-23.1	**2Ge**	54.0	-2.7
3Si	37.0	-31.0	**3Ge**	49.0	-8.7
4Si	38.6	-26.8	**4Ge**	49.6	-6.8
5Si	39.8	-28.4	**5Ge**	50.3	-7.2
8Si	49.1	-18.9	**8Ge**	59.3	3.1
9Si	54.2	-11.9	**9Ge**	66.5	11.1
14Si	43.4	-26.2	**14Ge**	54.6	-3.6

Activation of H_2 by CAAGes may need elevated reaction conditions as evident not only from the values of calculated reaction free energies which are significantly less exergonic (endergonic for **8Ge** and **9Ge**) but also from the computed activation barriers (49.0 – 66.5 kcal mol^{-1}) that are relatively higher than those computed for CAASis (Table 3.4). The relatively higher barrier heights obtained for CAAGes may be attributed to their reduced Lewis basicity (lower E_σ values, Figure 3.3) compared to that of CAASis. As in the case with CAASis, we observe similar increase in occupancies of the formally vacant 4p orbital at the Ge center in going from the ground to the transition states (Table 3.2 and Table 3.3).

[3.3.2] Activation of Ammonia

Activation of ammonia has been an active area of research over the years because of its wide application in various industrial processes [41]. For example, ammonia is used as a source of nitrogen for the production of various industrial amines, fertilizers, pharmaceutical products as well as inorganic acids etc [42]. However, it is to be noted that unlike dihydrogen activation, activation of ammonia by transition metal complexes is a challenging task as they tend to form classical Werner-type amine complexes over bond cleavage [42]. However, a number of silylenes or germylenes are known which can split NH_3 under ambient reaction conditions [43]. Thus, it may be rewarding to probe the reactivity of these amphiphilic CAASis and CAAGes towards activation of the N–H bond of NH_3.

The mechanism may be envisaged as comprising of two steps [40] as shown in Figure 3.7 for **1Si** and **1Ge** as representative examples. The optimized geometrical and electronic parameters for all the intermediates and TSs are listed in Table 3.5 and Table 3.6 and their optimized geometries are given in Figure 3.8 and Figure 3.9 respectively. In

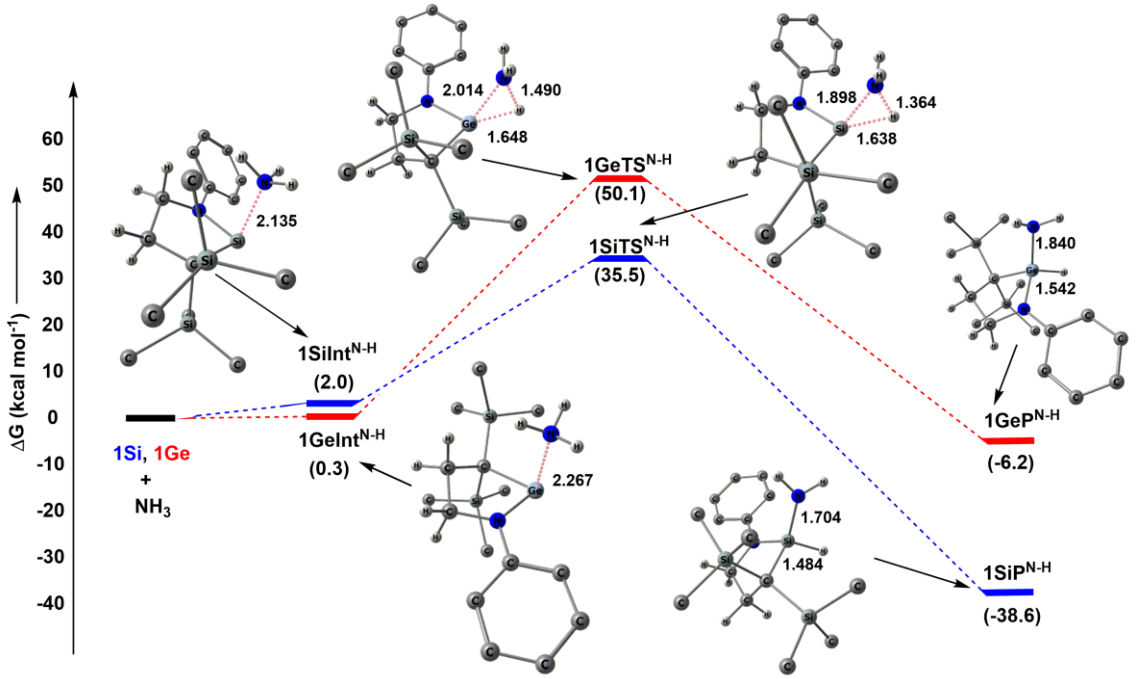

Figure 3.7: Reaction profile diagram for the activation of N–H bond of NH_3 by **1Si** and **1Ge** at M06-D3/def2-TZVP (Toluene) level of theory. The hydrogen atoms of the methyl and phenyl groups are omitted for the sake of clarity.

Table 3.5: Calculated (M06-D3/def2-TZVP (Toluene)) important geometrical parameters and natural charges at the nitrogen atom of NH_3 and Si/Ge center for the intermediate (**Int**) involved in the activation of N–H bond of NH_3 by CAASis (**1Si-5Si** and **14Si**), CAAGes (**1Ge-5Ge** and **14Ge**) and NacNacSi (**IIa**). Bond lengths are given in Å and Wiberg Bond Index (WBI) values are given within parentheses.

Molecules	H_3N–Si	q_{NH_3}	q_{Si}	Molecules	H_3N–Ge	q_{NH_3}	q_{Ge}
1SiInt^{N-H}	2.135 (0.344)	-1.013	1.021	**1GeInt^{N-H}**	2.267 (0.317)	-1.020	1.004
2SiInt^{N-H}	2.085 (0.366)	-1.026	0.985	**2GeInt^{N-H}**	2.304 (0.303)	-1.027	1.010
3SiInt^{N-H}	2.097 (0.356)	-1.024	1.016	**3GeInt^{N-H}**	2.349 (0.289)	-1.023	1.031
4SiInt^{N-H}	2.137 (0.335)	-1.031	1.040	**4GeInt^{N-H}**	2.369 (0.281)	-1.025	1.040
5SiInt^{N-H}	2.087 (0.371)	-1.029	1.009	**5GeInt^{N-H}**	2.317 (0.311)	-1.030	1.040
14SiInt^{N-H}	2.097 (0.360)	-1.013	0.935	**14GeInt^{N-H}**	2.310 (0.282)	-1.023	0.987
IIa-Int^{N-H}	2.141 (0.335)	-1.027	1.092				

the first step, the lone pair at the nitrogen atom (LP_N) of ammonia interacts with the vacant p_π orbital centered at the Si/Ge center, resulting in the formation of an intermediate (**1SiInt^{N-H}** and **1GeInt^{N-H}**, Figure 3.7). Thereafter, in the second step, the intermediates pass through a TS (**1SiTS^{N-H}** and **1GeTS^{N-H}**) involving barriers of 35.5 and 50.1 kcal mol^{-1} respectively to yield the N–H bond splitting products. The splitting of the N–H bond is assisted by interaction of the lone pair electron density from the Si/Ge center to one of the σ^*_{N-H} orbital thereby generating a pseudo amide fragment and a positively polarized hydrogen atom. The TSs, **1SiTS^{N-H}** and **1GeTS^{N-H}** exhibits significantly elongated and polarized N–H bond (Table 3.6) with the amide fragment being strongly bonded to the Si/Ge center while the hydrogen remain distant from the Si/Ge center. Both the pseudo amide fragment and the hydrogen eventually migrate to the Si/Ge center producing the N–H splitting product. In all the TSs, the NH_3 fragment is perfectly oriented for activation with one of the N–H bond aligning in the direction of the Si/Ge lone pair orbital. We observe a gradual and significant shortening of the

Si/Ge–N (NH_3) bonds all the way from the intermediates to the products through the respective TSs (Figure 3.7 and Tables 3.5–3.6).

Table 3.6: Calculated (M06-D3/def2-TZVP (Toluene)) important geometrical parameters and natural charges at the nitrogen atom of the pseudo amide fragment (q_{NH_2}) and hydrogen atom (q_H) of the transition states involved in the activation of N–H bond of NH_3 by CAASis (**1Si-5Si**, **8Si-9Si** and **14Si**), CAAGes (**1Ge-5Ge**, **8Ge-9Ge** and **14Ge**) and NacNacSi (**IIa**). Bond lengths (E – X, E = Si, Ge and X = N, C), bond angles (∠C-E-N) are given in Å and in degree (°) respectively.

Molecule	H_2N-H	E – H	$E-NH_2$	E - X	∠C-E-N	q_{NH_2}	q_H
1SiTS^{N-H}	1.364	1.638	1.898	1.761/1.892	94.5	-1.250	0.226
2SiTS^{N-H}	1.371	1.636	1.881	1.781/1.889	92.7	-1.244	0.226
3SiTS^{N-H}	1.336	1.652	1.881	1.766/1.888	96.1	-1.238	0.231
4SiTS^{N-H}	1.356	1.641	1.913	1.739/1.905	100.2	-1.258	0.222
5SiTS^{N-H}	1.373	1.628	1.871	1.778/1.892	93.2	-1.203	0.231
8SiTS^{N-H}	1.368	1.640	1.896	1.776/1.811	93.2	-1.242	0.197
9SiTS^{N-H}	1.377	1.644	1.889	1.791/1.824	91.4	-1.238	0.189
14SiTS^{N-H}	1.369	1.638	1.890	1.772/1.821	94.3	-1.234	0.207
IIa-TS^{N-H}	1.382	1.632	1.865	1.740/1.758	101.9	-1.237	0.212
1GeTS^{N-H}	1.490	1.648	2.014	1.889/1.982	90.8	-1.242	0.166
2GeTS^{N-H}	1.520	1.632	2.015	1.891/1.985	90.3	-1.237	0.160
3GeTS^{N-H}	1.514	1.636	2.012	1.878/1.981	93.1	-1.234	0.160
4GeTS^{N-H}	1.518	1.634	2.032	1.867/1.998	98.1	-1.240	0.157
5GeTS^{N-H}	1.513	1.637	1.993	1.890/1.987	90.4	-1.229	0.165
8GeTS^{N-H}	1.511	1.634	2.062	1.887/1.883	90.0	-1.257	0.142
9GeTS^{N-H}	1.515	1.649	2.046	1.899/1.898	88.5	-1.254	0.136
14GeTS^{N-H}	1.494	1.647	2.014	1.886/1.899	91.8	-1.247	0.151

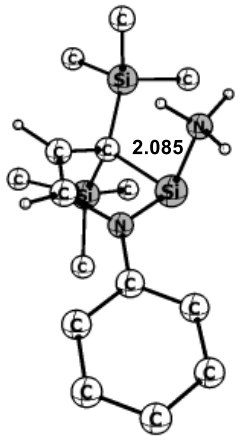

2SiInt^{N-H}

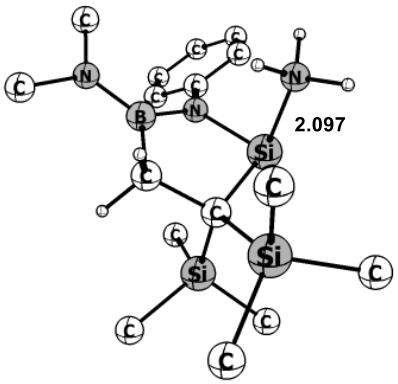

3SiInt^{N-H}

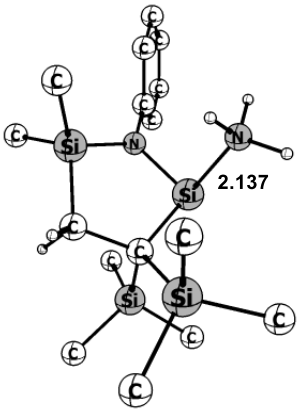

4SiInt^{N-H}

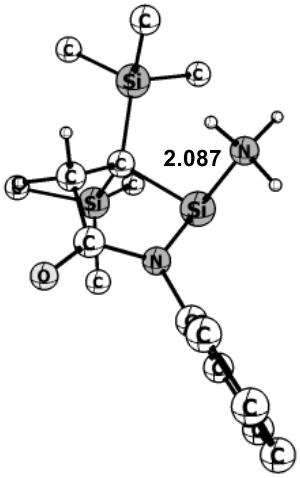

5SiInt^{N-H}

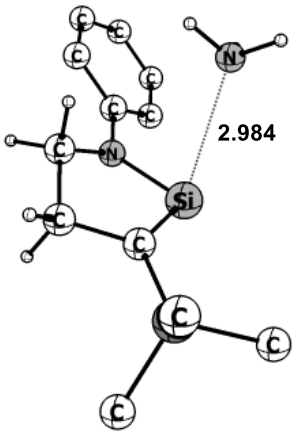

8SiInt^{N-H}

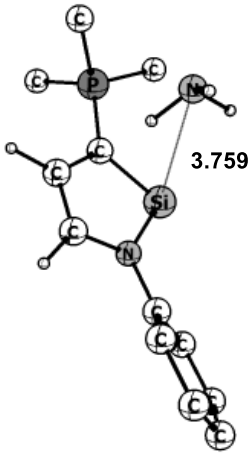

9SiInt^{N-H}

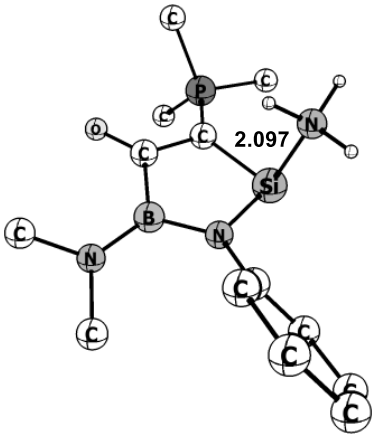

14SiInt^{N-H}

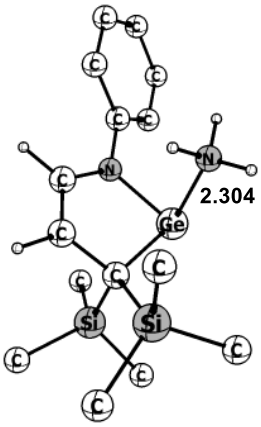

2GeInt^{N-H}

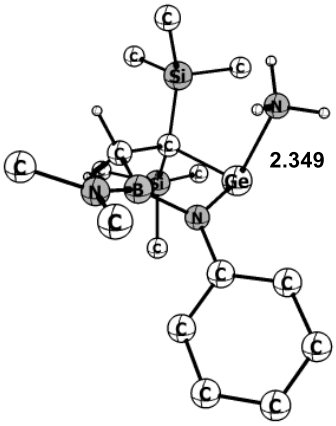

3GeInt^{N-H}

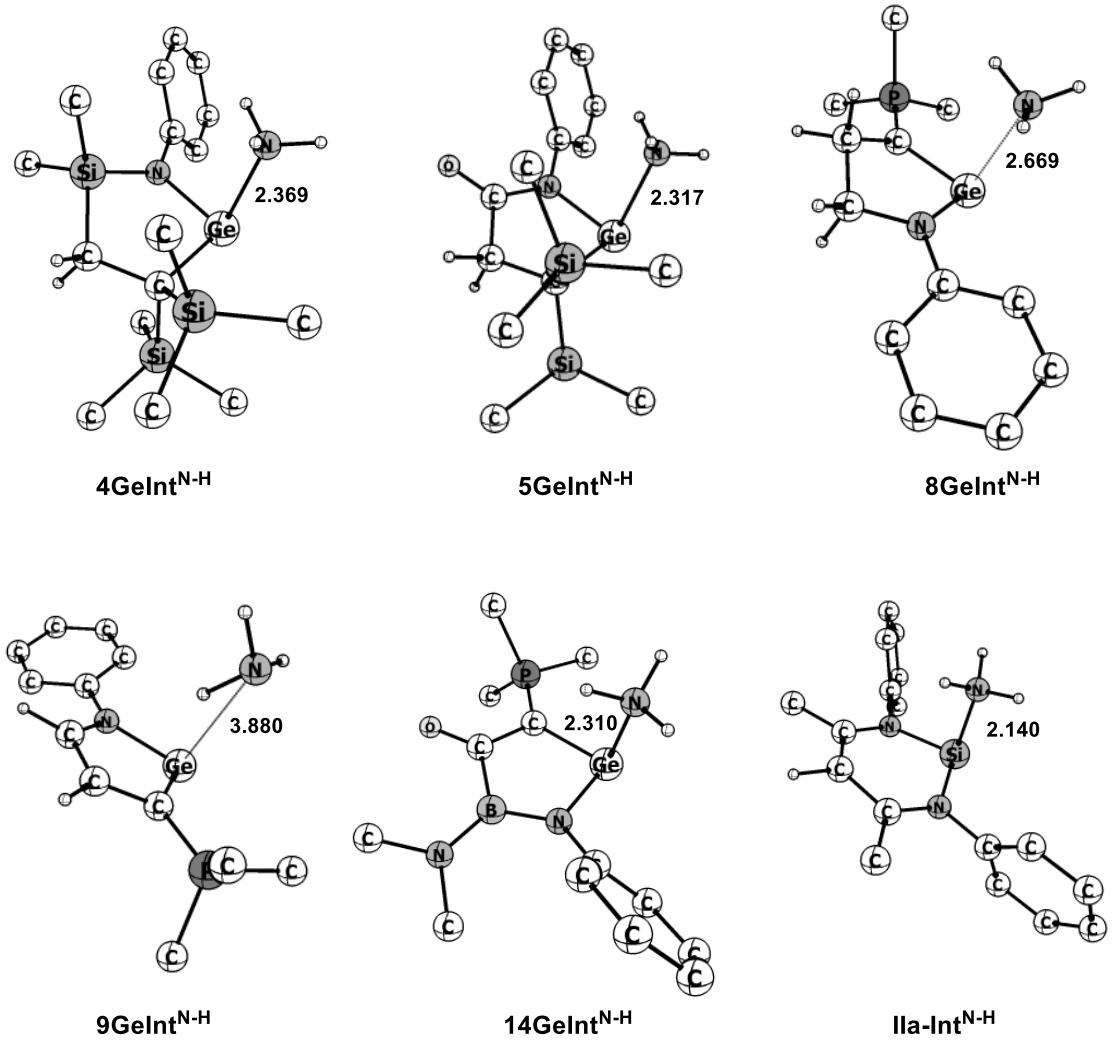

Figure 3.8: Optimized geometries for the intermediate (Int^{N-H}) involved in the activation of N–H bond of NH_3 by CAASis (**2Si-5Si**, **8Si-9Si** and **14Si**), CAAGes (**2Ge-5Ge**, **8Ge-9Ge** and **14Ge**) and NacNacSi (**IIa**) at M06-D3/def2-TZVP (Toluene) level of theory. The hydrogen atoms of the phenyl and methyl groups are omitted for clarity.

It can be ascertained from Table 3.7 that except the intermediates **5SiInt^{N-H}** and **5GeInt^{N-H}** formed by the strongly electrophilic **5Si** and **5Ge** that lies lower in energy (*ca.* 1.0 and 0.8 kcal mol^{-1}) than the starting reactants, all others lie at a slightly higher energy (0.3–5.2 kcal mol^{-1}). All the intermediates compute significantly stretched Si–N (2.085 – 2.137 Å) and Ge–N (2.267 – 2.369 Å) bond lengths but still maintains considerable interaction between the LP_N and the vacant p_π orbital at the Si/Ge center as evident from the calculated non-negligible values of WBI values (Table 3.5). It may be noted that due to their low π-acidity (Figure 3.3), compounds **8** and **9** could not form a stable intermediate with NH_3. However, considering their substantial Lewis basicity,

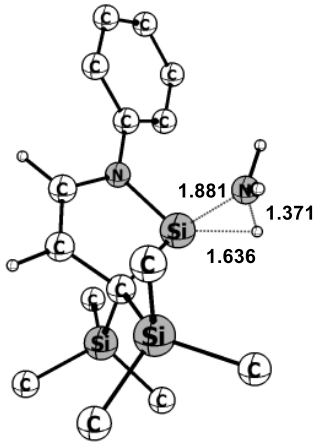

2SiTS^{N-H}

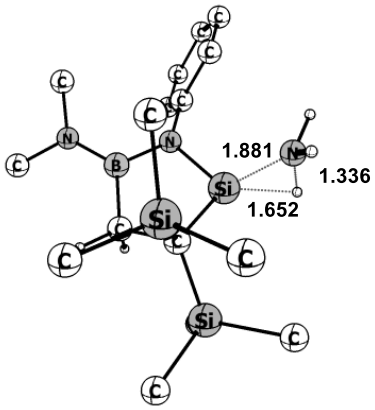

3SiTS^{N-H}

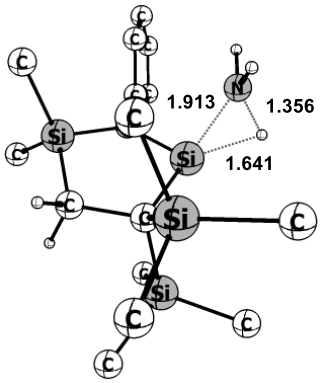

4SiTS^{N-H}

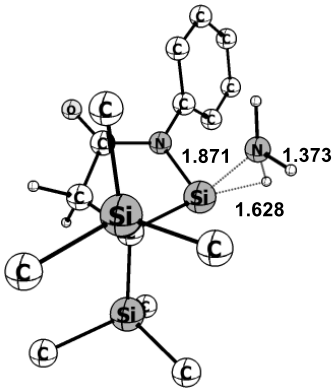

5SiTS^{N-H}

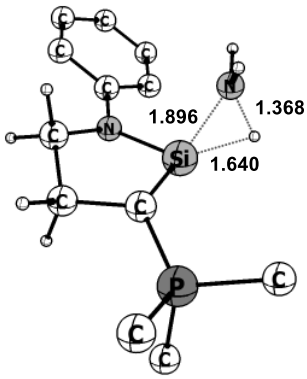

8SiTS^{N-H}

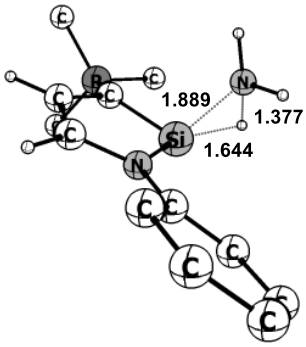

9SiTS^{N-H}

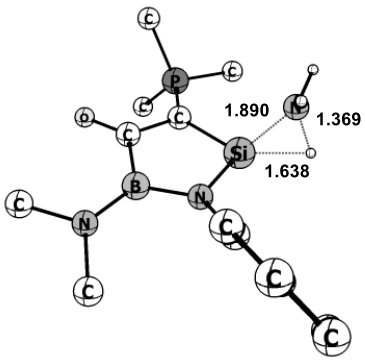

14SiTS^{N-H}

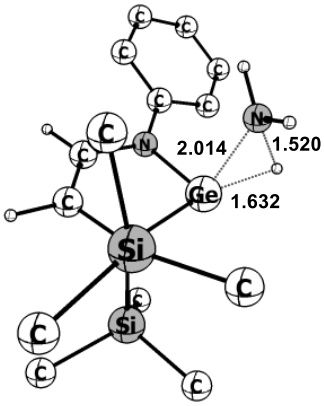

2GeTS^{N-H}

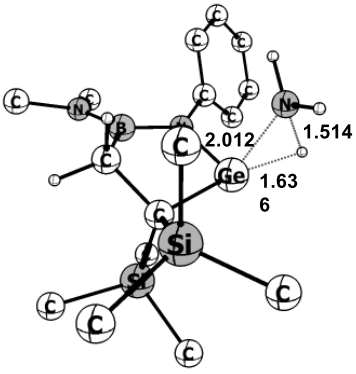

3GeTS^{N-H}

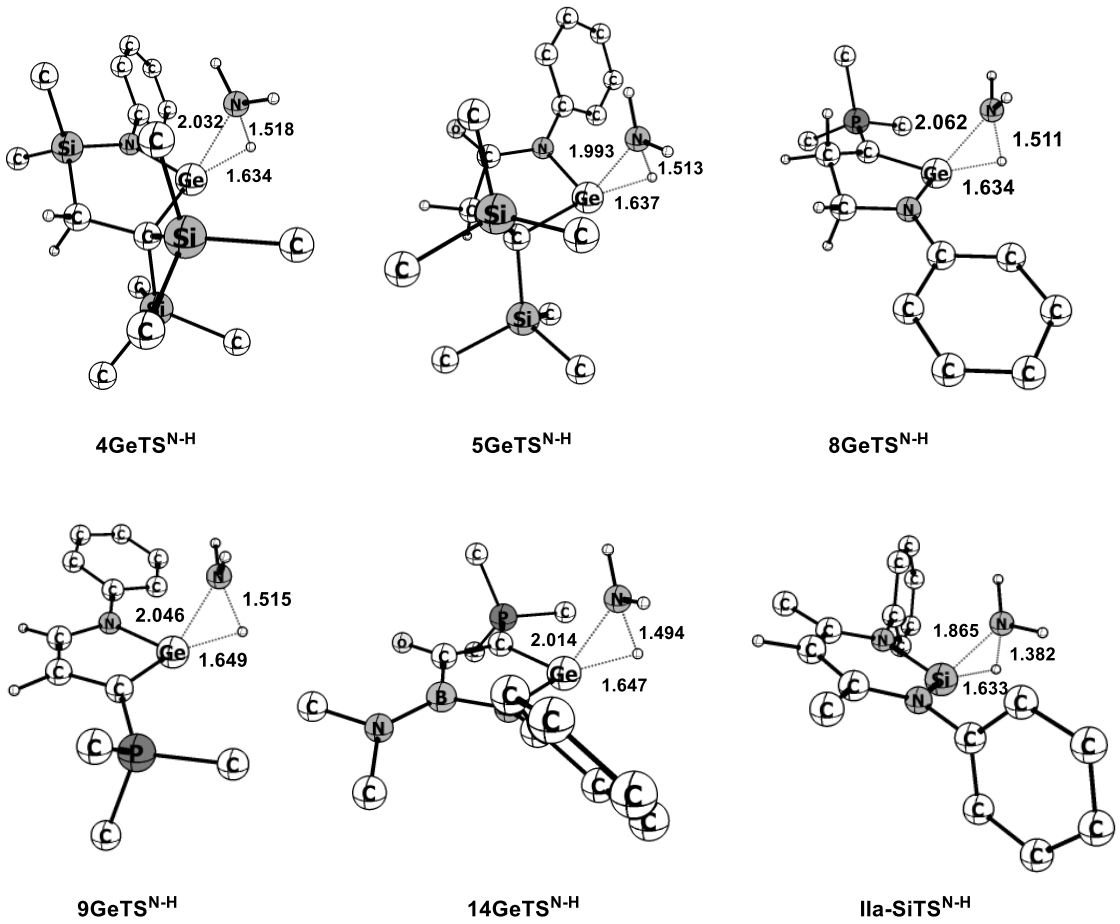

Figure 3.9: Optimized geometries for the transition states involved in the activation of N –H bond of NH_3 by CAASis (**2Si-5Si**, **8Si-9Si** and **14Si**), CAAGes (**2Ge-5Ge, 8Ge-9Ge** and **14Ge**) and NacNacSi (**IIa**) at M06-D3/def2-TZVP (Toluene) level of theory. The hydrogen atoms of the phenyl and methyl groups are omitted for clarity.

they should be able to activate ammonia in a manner similar to that of activation by strongly nucleophilic carbenes such as CAAC, i.e., the activation is initiated by interaction of the lone pair at Si/Ge center with one of the N–H antibonding orbital (σ^*_{N-H}) generating a pseudo amide like fragment [16].

The activation barriers ($\Delta G°_{TS^{N-H}}^{\ddagger}$) obtained for activation by CAASis fall in the range of 33.7–47.5 kcal mol^{-1} (Table 3.7) with the lowest being computed for **3Si** and **5Si**. It is encouraging to note that the barrier heights computed for these CAASis are either lower (**1Si**, **2Si**–**5Si** and **14Si**) or comparable (**2Si**) to that obtained for the experimentally evaluated NacNacSi **IIa** (38.4 kcal mol^{-1}, calculated at the same level of theory). Therefore, some of these newly designed CAASis (**2Si-5Si** and **14Si**) could be considered as suitable candidates for metal-free activation of ammonia. However,

Table 3.7: Calculated (M06-D3/def2-TZVP (Toluene)) activation energy barrier ($\Delta G°_{TS^{N-H}}‡$, kcal mol^{-1}), free energies of formation (in kcal mol^{-1}) of the intermediate ($\Delta G°_{Int^{N-H}}$) and N–H splitting product ($\Delta G°_{Total^{N-H}}$).

Molecules	$\Delta G°_{Int^{N-H}}$	$\Delta G°_{TS^{N-H}}‡$	$\Delta G°_{Total^{N-H}}$	Molecules	$\Delta G°_{Int^{N-H}}$	$\Delta G°_{TS^{N-H}}‡$	$\Delta G°_{Total^{N-H}}$
1Si	2.0	35.5	-38.6	**1Ge**	0.3	50.1	-6.2
2Si	2.4	38.2	-33.7	**2Ge**	1.8	52.6	0.1
3Si	2.1	33.7	-40.6	**3Ge**	3.2	46.7	-7.0
4Si	5.2	37.4	-36.1	**4Ge**	1.7	47.1	-6.1
5Si	-1.0	33.7	-38.7	**5Ge**	-0.8	49.3	-7.2
8Si	-	42.2	-31.6	**8Ge**	-	55.3	1.2
9Si	-	47.5	-24.6	**9Ge**	-	62.2	11.5
14Si	1.8	35.4	-38.5	**14Ge**	1.7	50.7	-5.7
IIa	1.8	38.4	-35.7				

despite possessing enhanced σ-basicity, the ylide decorated CAASis **8Si** and **9Si** compute considerably higher barrier than others which may be attributed to their lower π-acidity than others. Furthermore, the calculated reaction free energies ($\Delta G°_{Total^{N-H}}$) are found to be significantly exergonic (-24.6 to -40.6 kcal mol^{-1}, Table 3.7) indicating that N–H splitting by the CAASis are thermodynamically favourable.

On the other hand, the activation barriers computed for CAAGes (**1Ge-5Ge** and **14Ge**) are found to be significantly higher (Table 3.7) than those for CAASis (**1Si-5Si** and **14Si**) due to the considerably lower Lewis basicity of CAAGes as explained earlier (*vide supra*). The reaction free energies are also less exergonic. Thus, both the calculated barrier heights and reaction free energies indicate that CAAGes may need elevated reaction conditions for N–H splitting and this also perhaps explain why no 1,1–addition product is obtained to date with *N*-heterocyclic germylenes. Therefore, similar to the dihydrogen activation, once again CAASis turned out to be better candidates for the activation of ammonia than CAAGes.

[3.3.3] Activation of Toluene

A number of silylenes or germylenes are reported which are capable of activating enthalpically strong C–H bonds [44]. In this regard, it is worth mentioning the recent work of Iwamoto and co-workers who have shown the reactivity of **1Si** towards activation of inert C–H (sp^3) bond of toluene (CH_3Ph) [12]. Herein we have made an attempt to study the potential of these skeletally substituted CAASis and CAAGes towards the activation of toluene. The mechanism is similar to that of dihydrogen activation, i.e., the σ-symmetric lone pair orbital of the central Si/Ge atom of CAASis/CAAGes interacts with one of the C–H antibonding orbital (σ^*_{C-H}) thereby generating a pseudo anionic fragment ($PhCH_2$). Thereafter, the gradual migration of the $PhCH_2$ fragment from the activated C–H bond towards the vacant p_π orbital centered at the Si/Ge center yields the desired C–H bond cleaved product. The overall process proceeds via a TS in which the Si/Ge center interact simultaneously with the both the hydrogen and $PhCH_2$ fragment. Accordingly, we have searched for the probable TSs involved in the activation of toluene.

The complete reaction profile as well as optimized geometries of the TSs for insertion of CAASis into the benzylic C–H bond of toluene is illustrated in Figure 3.10 by considering **1Si** and **5Si** as representative examples. The important geometrical and electronic parameters for all the TSs are given in Table 3.8 and their geometries are given in Figure 3.11. All the TSs exhibit significantly elongated (1.609-1. 723 Å) and polarized (Table 3.8) C–H bond with the hydrogen being strongly bonded to the Si center (1.595 - 1.626 Å) while the $PhCH_2$ fragments remain distant from the Si center (2.105 - 2.171 Å). As observed for activation of H_2, the TSs for activation of toluene is also accompanied by an increase in occupancy of the formally vacant valence 3p orbital at the central Si atom. For example, the occupancies increase from 0.256 (**1Si**) and 0.182 (**5Si**) to 0.475 and 0.461 in **1SiTS^{C-H}** and **5SiTS^{C-H}** (Table 3.8) respectively.

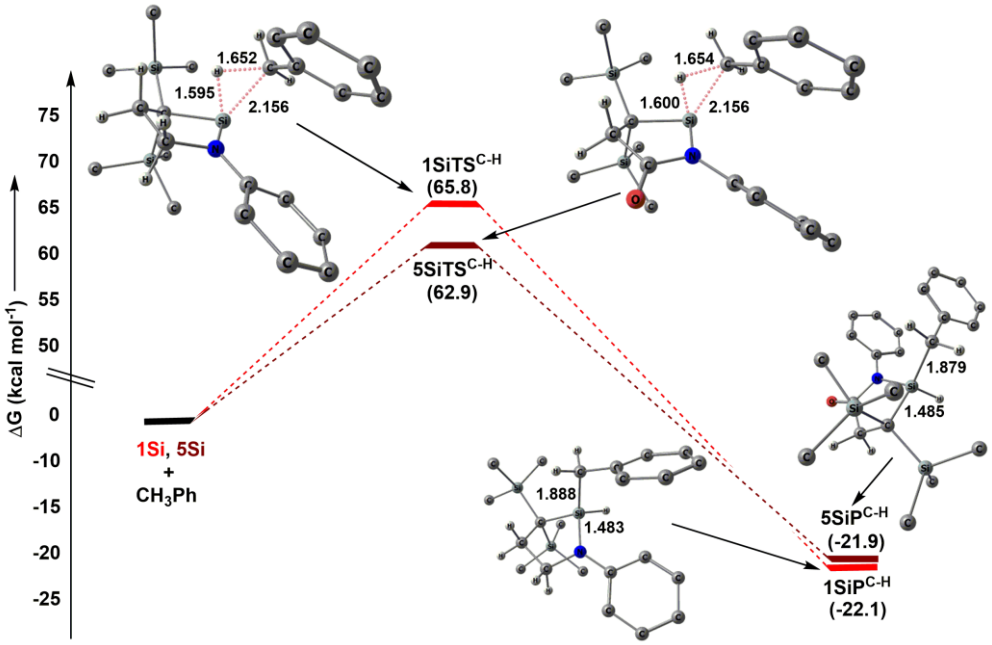

Figure 3.10: Reaction profile diagram for the activation of C–H bond of CH_3Ph by **1Si** and **5Si** at M06-D3/def2-TZVP (Toluene) level of theory. The hydrogen atoms of the methyl and phenyl groups are omitted for the sake of clarity.

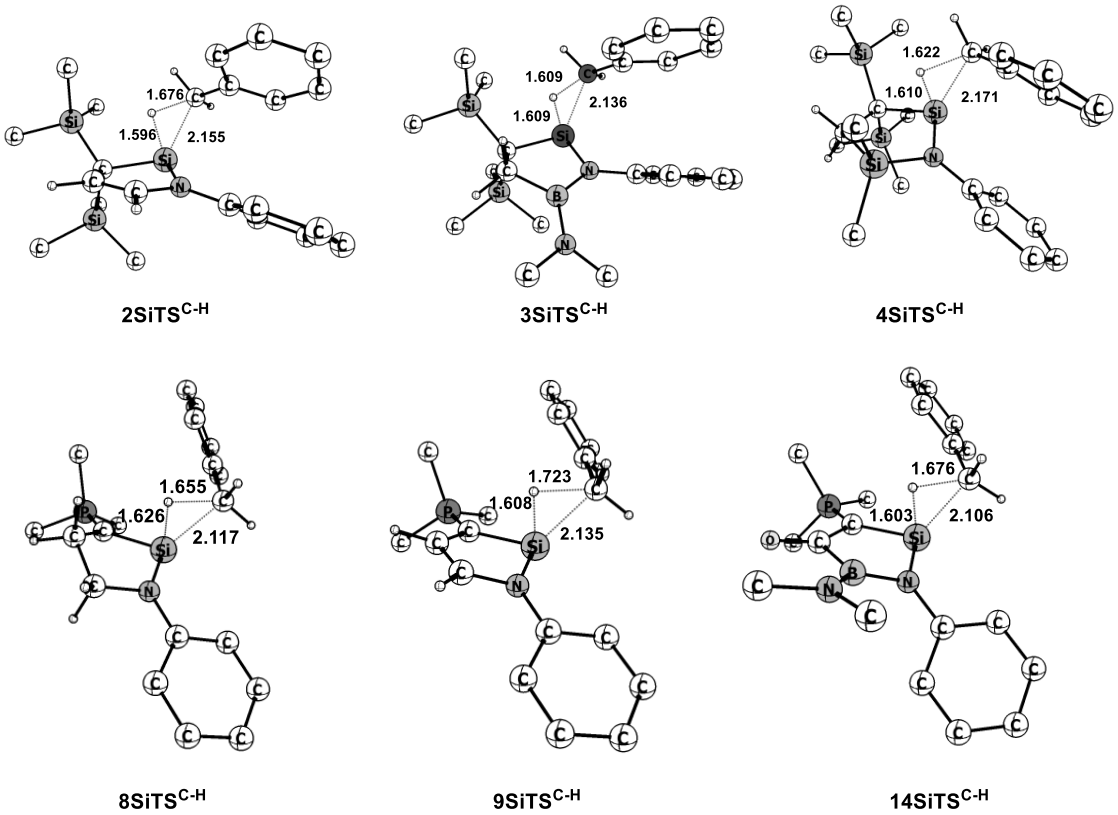

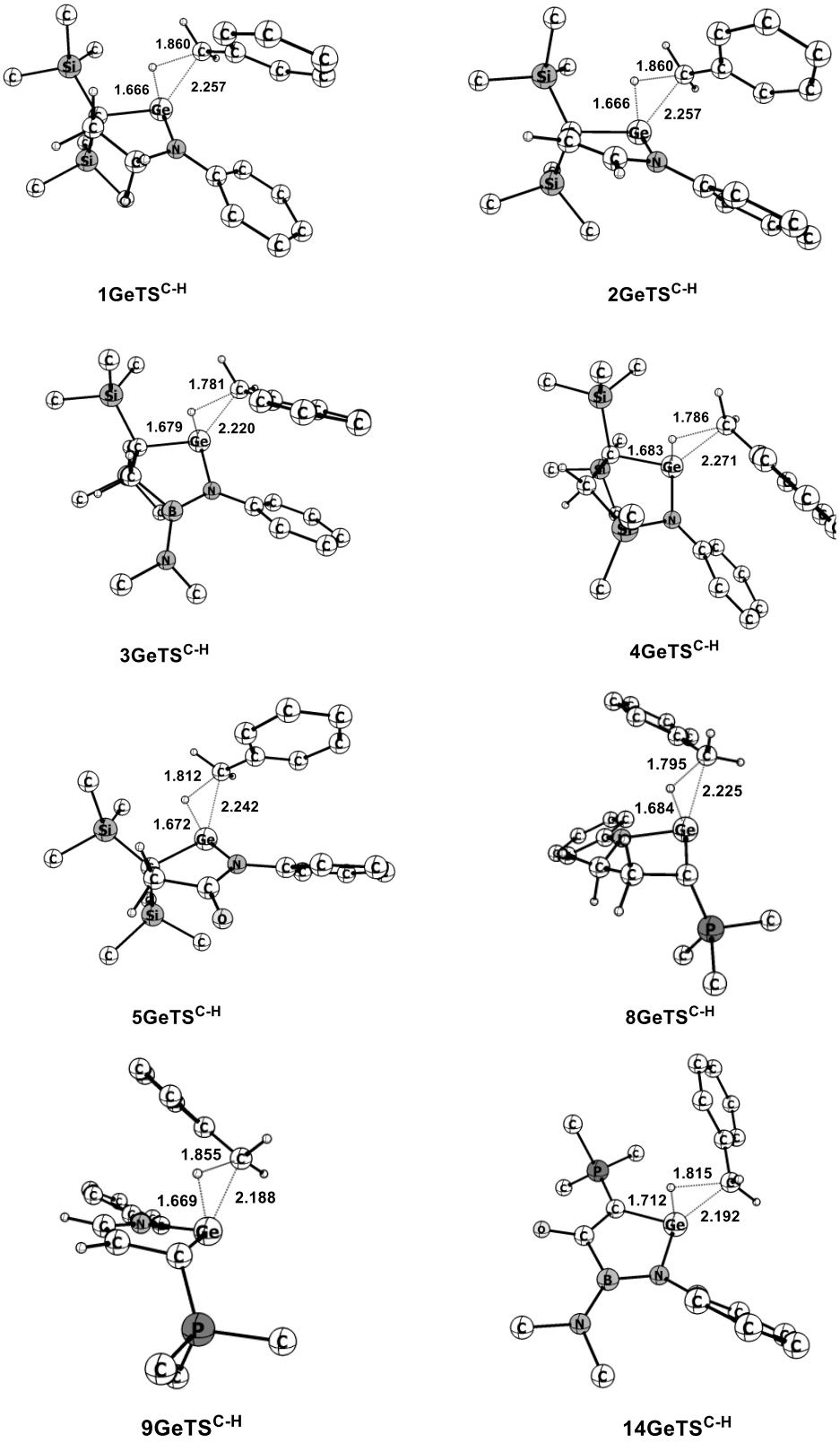

Figure 3.11: Optimized geometries for the transition states involved in the activation of C–H bond of CH_3Ph by CAASis (**2Si-4Si**, **8Si-9Si** and **14Si**) and CAAGes (**1Ge-5Ge**, **8Ge-9Ge** and **14Ge**) at M06-D3/def2-TZVP (Toluene) level of theory. The hydrogen atoms of the phenyl and methyl groups are omitted for clarity.

Table 3.8: Calculated (M06-D3/def2-TZVP (Toluene)) important geometrical parameters and natural charges at the carbon atom of the $PhCH_2$ fragment (q_{PhCH_2}) and hydrogen atom (q_H) and occupancies of the formally vacant p-orbital ($Occ_{Si/Ge}$) of the transition states involved in the activation of toluene by CAASis (**1Si-5Si**, **8Si-9Si** and **14Si**) and CAAGes (**1Ge-5Ge**, **8Ge-9Ge** and **14Ge**).

Molecule	$PhCH_2$–H	E–H	E–CH_2Ph	$Occ_{Si/Ge}$	q_{PhCH_2}	q_H
1SiTS^{C-H}	1.652	1.595	2.156	0.475	-0.570	0.066
2SiTS^{C-H}	1.676	1.596	2.155	0.524	-0.565	0.075
3SiTS^{C-H}	1.609	1.609	2.136	0.359	-0.616	0.093
4SiTS^{C-H}	1.622	1.610	2.171	0.431	-0.573	0.056
5SiTS^{C-H}	1.654	1.600	2.156	0.461	-0.562	0.063
8SiTS^{C-H}	1.655	1.626	2.117	0.963	-0.604	0.073
9SiTS^{C-H}	1.723	1.608	2.135	0.957	-0.576	0.066
14SiTS^{C-H}	1.676	1.603	2.105	0.461	-0.606	0.087
1GeTS^{C-H}	1.807	1.668	2.239	0.503	-0.500	0.030
2GeTS^{C-H}	1.860	1.666	2.257	0.542	-0.481	0.029
3GeTS^{C-H}	1.781	1.689	2.220	0.373	-0.540	0.052
4GeTS^{C-H}	1.786	1.683	2.271	0.477	-0.491	0.020
5GeTS^{C-H}	1.811	1.672	2.242	0.491	-0.490	0.028
8GeTS^{C-H}	1.795	1.684	2.224	0.382	-0.496	0.043
9GeTS^{C-H}	1.854	1.669	2.189	0.450	-0.550	0.081
14GeTS^{C-H}	1.815	1.712	2.192	0.863	-0.545	0.037

The barrier heights obtained for CAASis are found to be significantly high (62.9 – 82.6 kcal mol^{-1}, Table 3.9) and this explains the experimental observation of requirement of higher temperature for activation by **1Si**. It is indeed encouraging to note that some of the computationally designed CAASis (**3Si**–**5Si**) exhibits lower barriers compared to **1Si** and thus they could be ideal candidates for experimental realization. The unusually higher barrier obtained for **8Si** and **9Si** may be attributed to their significantly reduced π acidity compared to that of other CAASis (Figure 3.3) considered in this study for C–H activation.

Table 3.9: Calculated (M06-D3/def2-TZVP (Toluene)) activation energy barrier ($\Delta G°_{TS^{C-H}}‡$, kcal mol^{-1}) and reaction free energies ($\Delta G°_{Total^{C-H}}$, kcal mol^{-1}) for the activation of C – H bond of toluene by CAASis and CAAGes.

Molecules	$\Delta G°_{TS^{C-H}}‡$	$\Delta G°_{Total^{C-H}}$	Molecules	$\Delta G°_{TS^{C-H}}‡$	$\Delta G°_{Total^{C-H}}$
1Si	65.8	-22.1	**1Ge**	73.5	0.4
2Si	70.6	-16.7	**2Ge**	76.8	5.6
3Si	63.5	-23.3	**3Ge**	72.6	0.3
4Si	64.3	-21.2	**4Ge**	68.0	1.3
5Si	62.9	-21.9	**5Ge**	69.8	1.1
8Si	75.0	-13.5	**8Ge**	85.5	9.3
9Si	82.6	-5.6	**9Ge**	94.8	16.7
14Si	72.0	-21.6	**14Ge**	79.1	2.4

Further, a comparison of Tables 3.4 and Table 3.9 show that activation of toluene involve considerably higher barrier (*ca.* 23 – 29 kcal mol^{-1}) than that for H_2 activation which may be attributed to the fact that the computed transition state for toluene activation involves more steric hindrance than that for H_2 activation. The calculated reaction free energies ($\Delta G°_{Total^{C-H}}$) indicate possibility of the C–H activation process but may need higher temperatures as observed experimentally [12]. As expected, once again CAAGes compute much higher barrier (68.0-94.8 kcal mol^{-1}) than CAASis. Also, the calculated $\Delta G°_{Total^{C-H}}$ values are found to be endergonic in nature (0.4-16.7 kcal mol^{-1}, Table 3.9) indicating requirement of elevated reaction conditions in future synthetic endeavors toward C–H activations employing CAAGes.

[3.3.4] Activation of Triethylsilane

The recently discovered cyclic(alkyl)(amino)silylene **1Si** was found to insert into the Si–H bond of triethylsilane (Et_3SiH) upon heating at 100°C [12] which motivated us to probe the potential of some of the molecules considered in this work towards activation of Si–H bond. Conceptually, such an insertion process may proceed via two steps as shown in Figure 3.12 by considering **1Si** and **3Si** as representative examples [45]. In the first step, the silylene using its lone pair orbital forms a van der Waals complex

(featuring slightly activated Si–H bond) with $SiEt_3H$ which then passes through a TS to yield the Si–H scission product. The presence of an activated Si – H bond in the van der Waals complexes facilitates the Si – H bond splitting process. Further, for the sake of comparison, Kira's five-membered silylene (**IX**, Scheme 3.1) which is known to activate $SiEt_3H$ under ambient reaction conditions is also considered in this study [23].

The van der Waals complexes lie marginally higher in energy than the reactants (*ca.* 1.7-6.9 kcal mol^{-1}, Table 3.12) and they exhibit considerably elongated Si–$SiEt_3H$ bond lengths (Table 3.10 and Figure 3.13) that lie within the sum of van der Waals radii of Si (2.10 Å). As shown in Figure 3.12, the van der Waals complexes **1Si$_v$** and **3Si$_v$** pass through a TS (**1SiTS^{Si-H}** and **3SiTS^{Si-H}**) in which both the $SiEt_3$ fragments and the negatively polarized hydrogen atoms (Table 3.11 and Figure 3.14) simultaneously

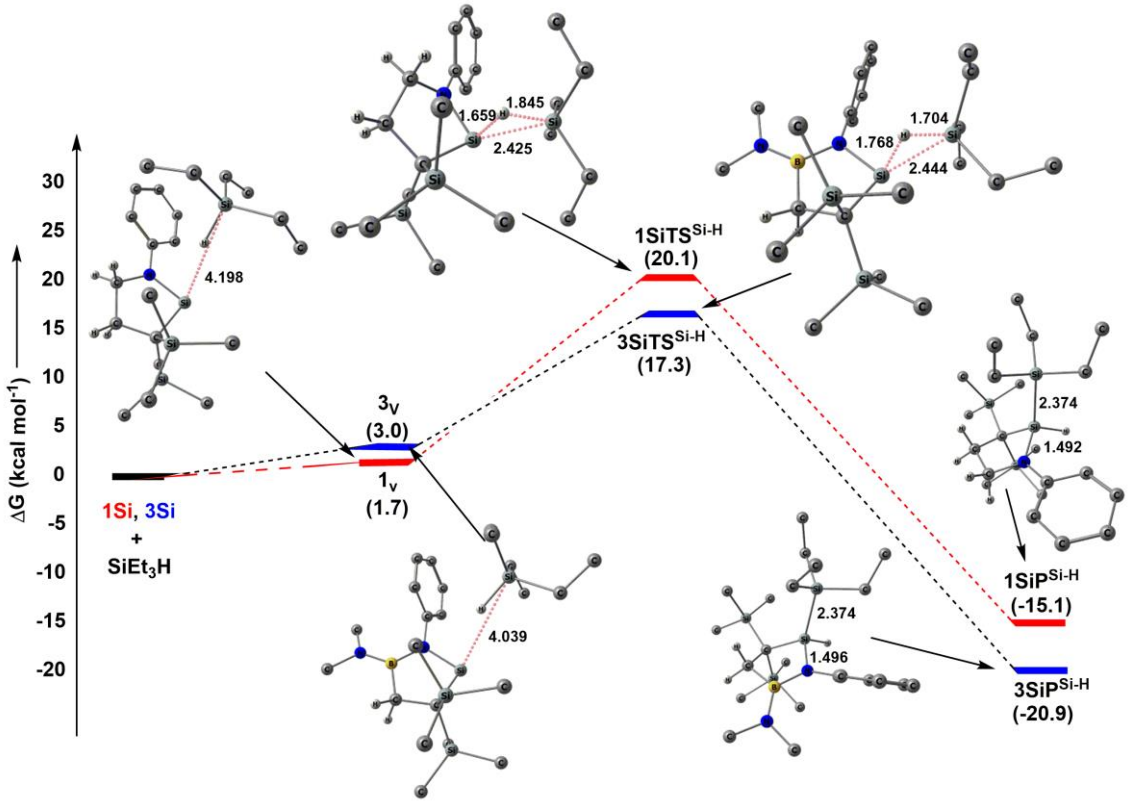

Figure 3.12: Reaction profile diagram for the activation of Si–H bond of $SiEt_3H$ by **1Si** and **3Si** at M06-D3/def2-TZVP (Toluene) level of theory. The hydrogen atoms of the methyl and phenyl groups are omitted for the sake of clarity.

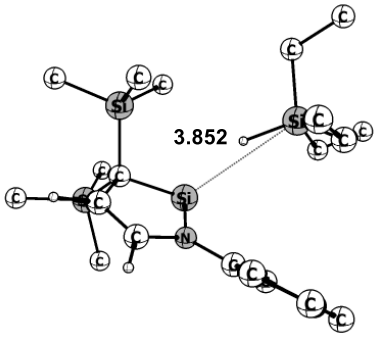

2Si$_v$

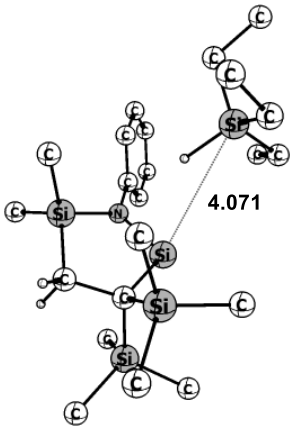

4Si$_v$

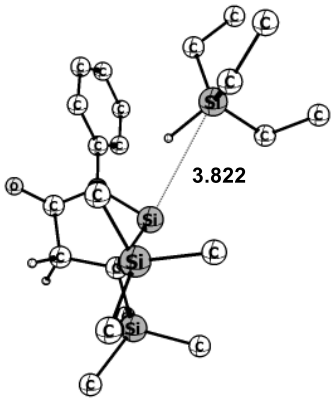

5Si$_v$

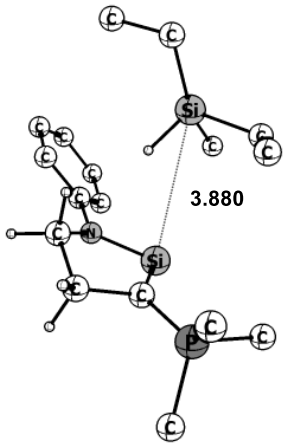

8Si$_v$

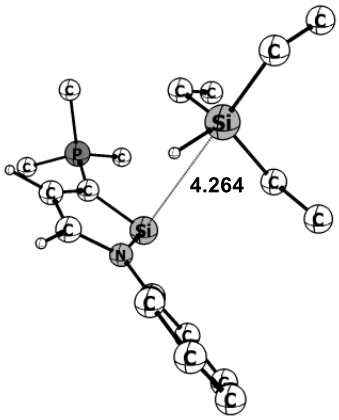

9Si$_v$

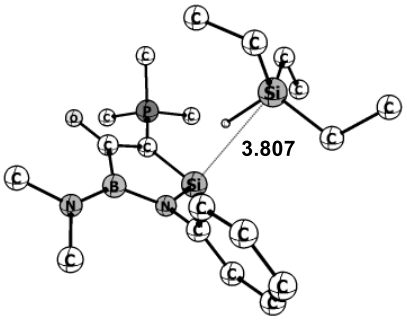

14Si$_v$

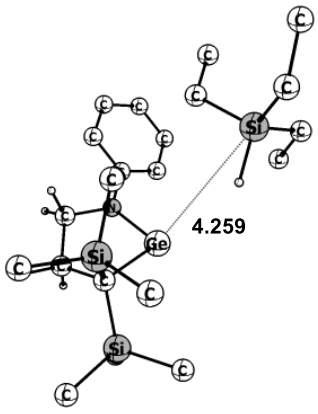

1Ge$_v$

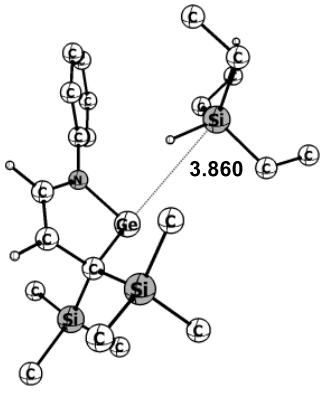

2Ge$_v$

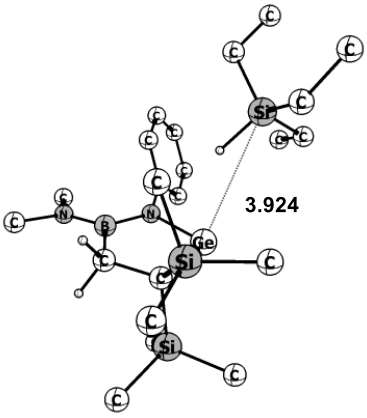

3Ge$_v$

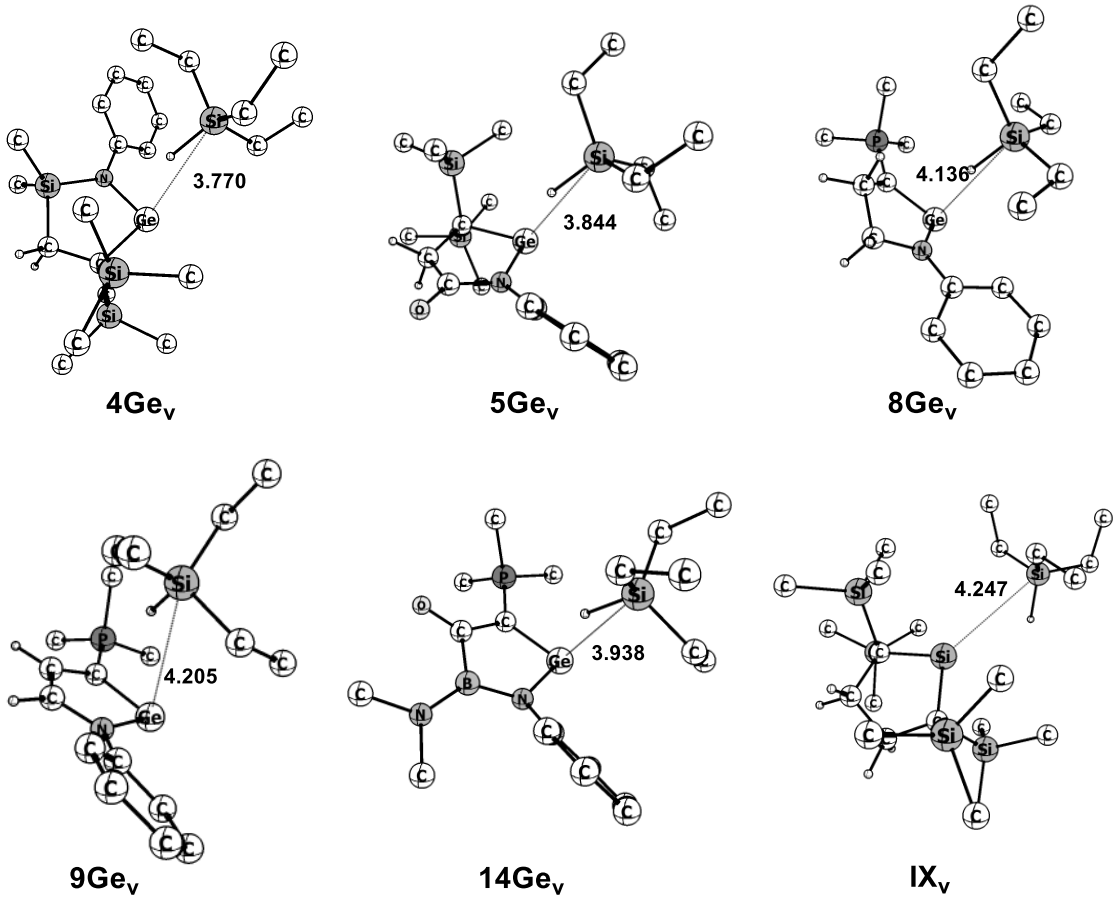

Figure 3.13: Optimized geometries for the van der Waals complexes involved in the activation of Si–H bond of $SiEt_3H$ by CAASis (**2Si-5Si**, **8Si-9Si** and **14Si**), CAAGes (**1Ge-5Ge**, **8Ge-9Ge** and **14Ge**) and **IX** at M06-D3/def2-TZVP (Toluene) level of theory. The hydrogen atoms of the methyl and phenyl rings are omitted for clarity.

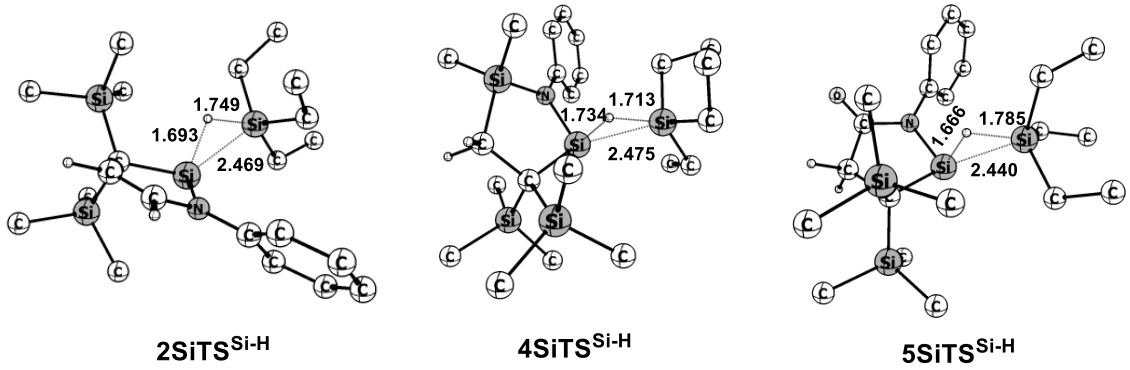

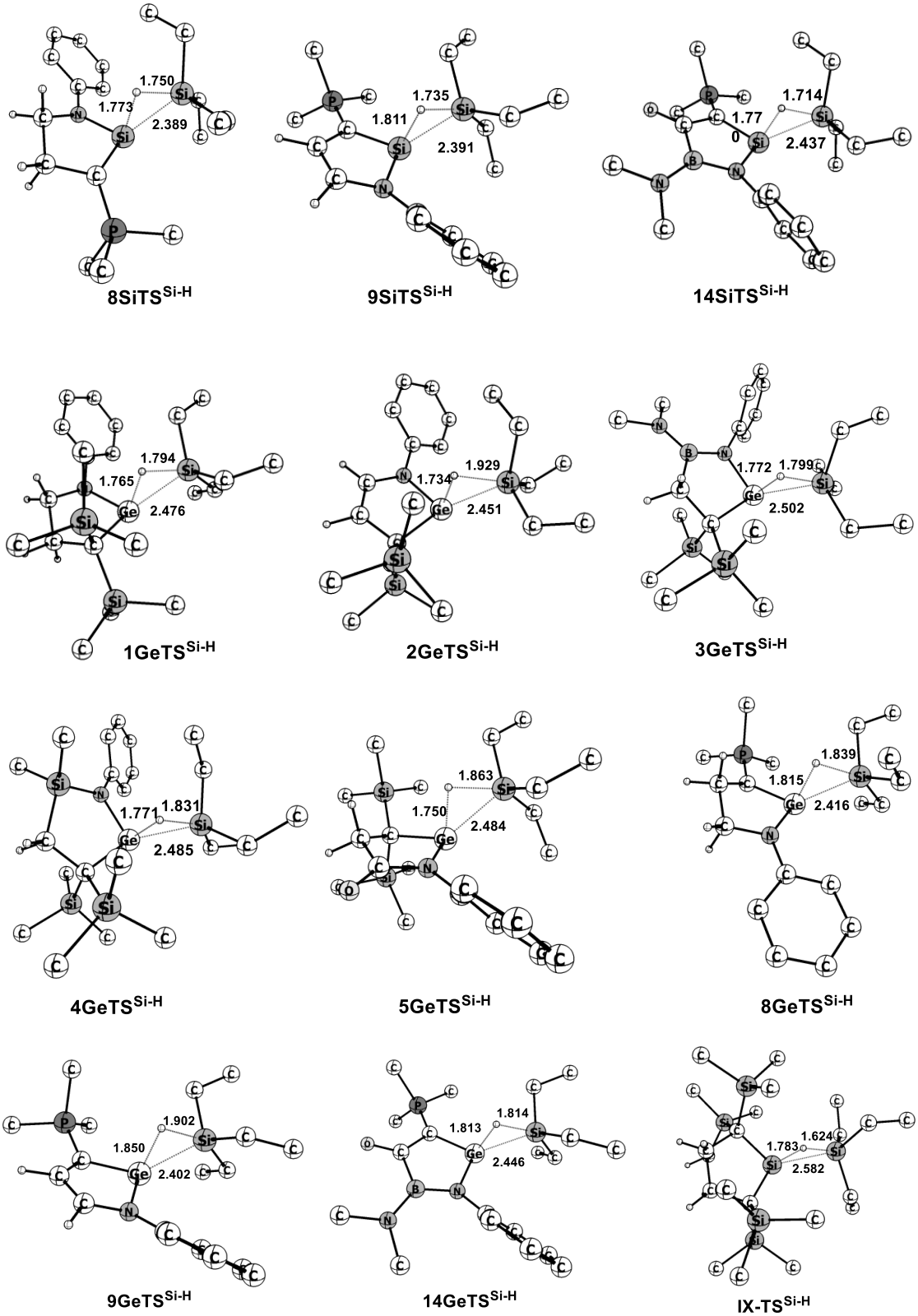

Figure 3.14: Optimized geometries for the transition states involved in the activation of Si–H bond of $SiEt_3H$ by CAASis (**2Si-5Si**, **8Si-9Si** and **14Si**), CAAGes (**1Ge-5Ge**, **8Ge-9Ge** and **14Ge**) and **IX** at M06-D3/def2-TZVP (Toluene) level of theory. The hydrogen atoms of the phenyl and methyl groups are omitted for clarity.

Table 3.10: Calculated (M06-D3/def2-TZVP (Toluene)) important geometrical parameters and natural charges at the silicon atom of the $SiEt_3H$ and at the central atom (E = Si, Ge) of the van der Waals complexes involved in the activation of Si-H bond of $SiEt_3H$ by CAASis (**1Si-5Si**, **8Si-9Si** and **14Si**), CAAGes (**1Ge-5Ge**, **8Ge-9Ge** and **14Ge**) and **IX**. The E-X (E = Si, Ge and X = C, N), Si – E bond lengths and ∠C – E – N bond angles (∠C-E-N, E = Si, Ge) are given in Å and in degree (°) respectively.

Molecule	$Et_3HSi - E$	E - X	∠C-E-N	q_{SiEt_3H}	q_E
$1Si_v$	4.198	1.749/1.903	91.3	1.498	1.155
$2Si_v$	3.852	1.775/1.904	89.0	1.516	1.103
$3Si_v$	4.039	1.759/1.898	93.2	1.515	1.192
$4Si_v$	4.071	1.738/1.912	97.0	1.494	1.211
$5Si_v$	3.822	1.773/1.895	90.6	1.514	1.210
$8Si_v$	3.880	1.787/1.796	89.9	1.477	0.947
$9Si_v$	4.264	1.803/1.823	87.2	1.458	0.777
$14Si_v$	3.807	1.787/1.825	92.2	1.512	1.035
IX_v	4.247	1.903/1.903	92.9	1.453	1.246
$1Ge_v$	4.259	1.873/2.013	87.5	1.463	1.079
$2Ge_v$	3.860	1.891/2.007	85.5	1.486	1.002
$3Ge_v$	3.924	1.880/2.009	90.1	1.509	1.097
$4Ge_v$	3.770	1.881/2.023	93.9	1.523	1.095
$5Ge_v$	3.844	1.899/2.003	87.2	1.514	1.118
$8Ge_v$	4.136	1.908/1.890	86.2	1.470	0.907
$9Ge_v$	4.205	1.932/1.914	83.9	1.453	0.764
$14Ge_v$	3.938	1.916/1.912	88.7	1.487	1.002

Table 3.11: Calculated (M06-D3/def2-TZVP (Toluene)) important geometrical parameters and natural charges at the silicon atom of the $SiEt_3$ fragment (q_{SiEt3}) and hydrogen atom (q_H) of the transition states involved in the activation of Si–H bond of $SiEt_3H$ by CAASis (**1Si-5Si**, **8Si-9Si** and **14Si**), CAAGes (**1Ge-5Ge**, **8Ge-9Ge** and **14Ge**) and **IX**.

Molecule	$Et_3Si–H$	E–H	$E–SiEt_3$	q_{SiEt3}	q_H
1SiTS^{Si-H}	1.845	1.659	2.425	1.522	-0.186
2SiTS^{Si-H}	1.749	1.693	2.469	1.527	-0.178
3SiTS^{Si-H}	1.704	1.768	2.444	1.348	-0.259
4SiTS^{Si-H}	1.713	1.734	2.475	1.497	-0.189
5SiTS^{Si-H}	1.785	1.669	2.440	1.545	-0.177
8SiTS^{Si-H}	1.750	1.773	2.389	1.397	-0.184
9SiTS^{Si-H}	1.735	1.810	2.390	1.381	-0.195
14SiTS^{Si-H}	1.714	1.770	2.437	1.427	-0.171
IX-TS^{Si-H}	1.624	1.783	2.582	1.536	-0.193
1GeTS^{Si-H}	1.794	1.765	2.476	1.504	-0.164
2GeTS^{Si-H}	1.929	1.733	2.451	1.540	-0.151
3GeTS^{Si-H}	1.799	1.772	2.502	1.509	-0.159
4GeTS^{Si-H}	1.831	1.771	2.485	1.527	-0.167
5GeTS^{Si-H}	1.863	1.750	2.484	1.542	-0.154
8GeTS^{Si-H}	1.839	1.815	2.416	1.412	-0.185
9GeTS^{Si-H}	1.902	1.850	2.403	1.420	-0.215
14GeTS^{Si-H}	1.814	1.813	2.446	1.453	-0.168

interacts with the silylene center. This is followed by the eventual migration of the $SiEt_3$ fragment and the H atom from the activated Si–H bond towards the Si center to yield the Si–H splitting product. The intramolecular charge transfer in the TSs is further

corroborated from the presence of significant negative charge at the H atom of $SiEt_3H$ (-0.171 to -0.259 and -0.151 to -0.215 for CAASis and CAAGes respectively, Table 3.11). The barrier heights ($\Delta G°_{TS^{Si-H}}‡$) obtained for the CAASis lie within the range of 17.3-37.0 kcal mol^{-1} with the highest and lowest barrier being computed for **9Si** and **3Si** respectively (Table 3.12). Furthermore, it may be noted that except **9Si**, all others compute comparable $\Delta G°_{TS^{Si-H}}‡$ values to that of the experimentally evaluated **1Si** implying that majority of these newly designed CAASis could be considered as potential candidates for activation of silanes. It is worth mentioning that the boron substituted CAASi **3Si** consistently outperforms the synthetically achievable **1Si** in all these bond activation processes considered in the present study. In addition, the reaction free energies are found to be significantly exergonic implying the feasibility of the reaction. Gratifyingly, the $\Delta G°_{TS^{Si-H}}‡$ values for activation by CAASis (except **9Si**) are found to be comparable with that computed for the experimentally evaluated Kira's five-membered silylene (**IX**, $\Delta G°_{TS^{Si-H}}‡$ = 24.3 kcal mol^{-1}, Table 3.12) thereby bolstering their potential towards activation of silanes.

Table 3.12: Calculated (M06-D3/def2-TZVP (Toluene)) activation energy barrier ($\Delta G°_{TS^{Si-H}}‡$, kcal mol^{-1}) and reaction free energies (kcal mol^{-1}) for the formation of the van der Waals complexes ($\Delta G°_{Int^{Si-H}}$) and Si–H splitting products ($\Delta G°_{Total^{Si-H}}$) by CAASis and CAAGes.

Molecule	$\Delta G°_{Int^{Si-H}}$	$\Delta G°_{TS^{Si-H}}‡$	$\Delta G°_{Total^{Si-H}}$	**Molecule**	$\Delta G°_{Int^{Si-H}}$	$\Delta G°_{TS^{Si-H}}‡$	$\Delta G°_{Total^{Si-H}}$
1Si	1.7	20.1	-15.1	**1Ge**	3.7	29.8	-2.2
2Si	3.8	26.4	-7.9	**2Ge**	3.1	34.4	7.4
3Si	3.0	17.3	-20.9	**3Ge**	2.2	28.3	-2.4
4Si	3.2	20.5	-14.4	**4Ge**	1.6	25.9	-3.4
5Si	6.9	23.2	-16.7	**5Ge**	3.3	25.4	-4.1
8Si	2.9	27.2	-7.4	**8Ge**	3.7	36.3	9.5
9Si	4.3	37.0	-0.8	**9Ge**	4.2	44.4	16.3
14Si	4.4	24.5	-11.9	**14Ge**	3.5	30.6	1.5
IX	6.3	24.3	-15.8				

Similar to the activation of H–H, N–H and C–H bonds, once again all the CAAGes compute considerably higher $\Delta G°_{TS^{Si\text{-}H}}{}^{\ddagger}$ values (25.4 – 44.4 kcal mol^{-1}) than those obtained for the CAASis (Table 3.12). This in part explains why till date no cyclic germylenes are known to activate silanes even though there may be other factors. In addition, the reaction free energies computed for the CAAGes are also found to be less negative compared to the CAASis indicating that all of them may demand elevated reaction condition for the activation of silanes.

[3.4] Conclusions

Density functional theory calculations performed on a number of skeletally substituted cyclic alkyl amino silylenes (CAASis) and germylenes (CAAGes) show that they compute significantly higher or comparable singlet-triplet separation ($\Delta E_{S\text{-}T}$) than their synthetically accessible parent analogues implying that all of them may be stable enough for experimental realization. Furthermore, some of the computationally designed CAASis and CAAGes are probed towards activation of H–H, N–H, C–H and Si–H bonds and the energetics of these reactions are compared with those of the experimentally evaluated systems including Driess's NacNac stabilized silylene (**IIa**) and Kira's five-membered silylene (**IX**). Our study successfully explains many of the experimental observations, e.g., requirement of higher temperature for C–H and Si–H bond activations. The activation barrier obtained for some of the CAASis in NH_3 activation are either found to be comparable or lower than that for the synthetically evaluated Driess's silylene indicating their potential in the activations of N–H bonds. Based on the calculated energy barrier for all the bond activations considered here, it may be concluded that these activation processes may need elevated reaction conditions. Further, C–H activation is found to be the most challenging one which is in agreement with experimental observations. Activations employing the heavier germylenes are calculated to have higher barriers indicating requirement of significantly elevated reaction conditions than those employing CAASis. We hope that our conclusion of many of the skeletally substituted CAASis considered here as promising candidates for small molecule activations will inspire synthetic chemists not only towards their experimental isolation but also their possible use as promoters of metal-free bond activations.

A comparison of the ligand properties of the group 14 carbenoids (MNHCs, CAASis and CAAGes) considered in this study reveals that the MNHCs exhibit

substantially higher electron donation ability compared to those of the CAASis/CAAGes. Since the primary interaction involved in the activation of σ-bonds by group 14 carbenoids is the transfer of electron density from the lone pair localized at the ene (C, Si and Ge) center to the σ*-antibonding orbital therefore, the MNHCs are expected to perform better than those of the CAASis/CAAGes. Indeed, the MNHCs compute considerably lower barrier heights as well as exergonic reaction free energies in different σ-bonds activation process.

[3.5] Bibliography

[1] Denk, M., Lennon, R., Hayashi, R., West, R., Belyakov, A. V., Verne, H. P., Haaland, A., Wagner, M., and Metzler, N. Synthesis and Structure of a Stable Silylene. *Journal of the American Chemical Society*, 116(6):2691-2692, 1994.

[2] Meller, A., and Gräbe, C. P. Synthese und Isolierung neuer Germanium(II)-Verbindungen und freier Germylene. *Chemische Berichte*, 118(5):2020-2029, 1985.

[3] (a) Gaspar, P. P., Xiao, M., Pae, D. H., Berger, D. J., Haile, T., Chen, T., Lei, D., Winchester, W. R., and Jiang, P. The quest for triplet ground state silylenes. *Journal of Organometallic Chemistry*, 646(1-2):68-79, 2002; (b) Lee, V. Y., and Sekiguchi, A. (2010). *Organometallic Compounds of Low-Coordinate Si, Ge, Sn and Pb: From Phantom Species to Stable Compounds*, John Wiley & Sons, pages.139-197.

[4] (a) Gehrhus, B., and Lappert, M. F. Chemistry of thermally stable bis(amino)silylenes. *Journal of Organometallic Chemistry*, 617-618:209-223, 2001; (b) Gehrhus, B., Lappert, M. F., Heinicke, J., Boese, R., and Bläser, D. Synthesis, structures and reactions of new thermally stable silylenes. *Journal of the Chemical Society, Chemical Communications*, (19):1931-1932, 1995.

[5] Haaf, M., Schmedake, T. A., and West, R. Stable Silylenes. *Accounts of Chemical Research*, 33(10):704-714, 2000.

[6] Ullah, F., Kühl, O., Bajor, G., Veszprémi, T., Jones, P. G., and Heinicke, J. Transition Metal Complexes of N-Heterocyclic Germylenes. *European Journal of Inorganic Chemistry*, 2009(2):221-229, 2009.

[7] Driess, M., Yao, S., Brym, M., van Wüllen, C., and Lentz, D. A New Type of N-Heterocyclic Silylene with Ambivalent Reactivity. *Journal of the American Chemical Society*, 128(30):9628-9629, 2006.

[8] Driess, M., Yao, S., Brym, M., and van Wüllen, C. A Heterofulvene-Like Germylene with a Betain Reactivity. *Angewandte Chemie International Edition*, 45(26):4349-4352, 2006.

[9] Jana, A., Schulzke, C., and Roesky, H. W. Oxidative Addition of Ammonia at a Silicon(II) Center and an Unprecedented Hydrogenation Reaction of Compounds with Low-Valent Group 14 Elements Using Ammonia Borane. *Journal of the American Chemical Society*, 131(13):4600-4601, 2009.

[10] Schoeller, W. W. Autocatalytic degradation of white phosphorus with silylenes. *Physical Chemistry Chemical Physics*, 11(26):5273-5280, 2009.

[11] (a) Yao, S., Brym, M., van Wüllen, C., and Driess, M. From a Stable Silylene to a Mixed-Valent Disiloxane and an Isolable Silaformamide–Borane Complex with Considerable Silicon–Oxygen Double-Bond Character. *Angewandte Chemie International Edition*, 46(22):4159-4162, 2007; (b) So, C. W., Roesky, H. W., Magull, J., and Oswald, R. B. Synthesis and Characterization of $[PhC(NtBu)_2]SiCl$: A Stable Monomeric Chlorosilylene. *Angewandte Chemie International Edition*, 45(24):3948-3950, 2006; (c) Sen, S. S., Jana, A., Roesky, H. W., and Schulzke, C. A Remarkable Base-Stabilized Bis(silylene) with a Silicon(I)–Silicon(I) Bond. *Angewandte Chemie International Edition*,48(45): 8356-8358, 2009; (d) Gau, D., Rodriguez, R., Kato, T., Saffon-Merceron, N., de Cózar, A., Cossío, F. P., and Baceiredo, A. Synthesis of a Stable Disilyne Bisphosphine Adduct and Its Non-Metal-Mediated CO_2 Reduction to CO. *Angewandte Chemie International Edition*, 50(5):1092-1096, 2011; (e) Wang, W., Inoue, S., Yao, S., and Driess, M. An Isolable Bis-Silylene Oxide ("Disilylenoxane") and Its Metal Coordination. *Journal of the American Chemical Society*, 132(45):15890-15892, 2010.

[12] Kosai, T., Ishida, S., and Iwamoto, T. A Two-Coordinate Cyclic (Alkyl)(amino)silylene: Balancing Thermal Stability and Reactivity. *Angewandte Chemie International Edition*, 55(50):15554-15558, 2016.

[13] Wang, L., Lim, Y. S., Li, Y., Ganguly, R., and Kinjo, R. Isolation of a Cyclic (Alkyl)(amino)germylene. *Molecules*, 21(8):990, 2016.

[14] Lavallo, V., Canac, Y., Präsang, C., Donnadieu, B., and Bertrand, G. Stable Cyclic (Alkyl)(Amino) Carbenes as Rigid or Flexible, Bulky, Electron-Rich Ligands for Transition-Metal Catalysts: A Quaternary Carbon Atom Makes the Difference. *Angewandte Chemie International Edition*, 44(35):5705-5709, 2005.

[15] Soleilhavoup, M., and Bertrand, G. Cyclic(Alkyl)(Amino)Carbenes (CAACs): Stable Carbenes on the Rise. *Accounts of Chemical Research*, 48(2):256-266, 2015.

[16] Frey, G. D., Lavallo, V., Donnadieu, B., Schoeller, W. W., and Bertrand, G. Facile Splitting of Hydrogen and Ammonia by Nucleophilic Activation at a Single Carbon Center. *Science*, 316(5823):439-441, 2007.

[17] Lavallo, V., Canac, Y., Donnadieu, B., Schoeller, W. W., and Bertrand, G. CO Fixation to Stable Acyclic and Cyclic Alkyl Amino Carbenes: Stable Amino Ketenes with a Small HOMO–LUMO Gap. *Angewandte Chemie International Edition*, 45(21):3488-3491, 2006.

[18] Frey, G. D., Masuda, J. D., Donnadieu, B., and Bertrand, G. Activation of Si–H, B–H, and P–H Bonds at a Single Nonmetal Center. *Angewandte Chemie International Edition*, 122(49):9444-9447, 2010.

[19] Asay, M., Inoue, S., and Driess, M. Aromatic Ylide-Stabilized Carbocyclic Silylene. *Angewandte Chemie International Edition*, 50(41):9589-9592, 2011.

[20] Alvarado-Beltran, I., Baceiredo, A., Saffon-Merceron, N., Branchadell, V., and Kato, T. Cyclic Amino(Ylide)Silylene: A Stable Heterocyclic Silylene with Strongly Electron-Donating Character. *Angewandte Chemie International Edition*, 55(52):16141-16144, 2016.

[21] Del Rio, N., Baceiredo, A., Saffon-Merceron, N., Hashizume, D., Lutters, D., Müller, T., and Kato, T. A Stable Heterocyclic Amino(phosphanylidene-σ^4-phosphorane) Germylene. *Angewandte Chemie International Edition*, 55(15):4753-4758, 2016.

[22] Kira, N., Ishida, S., Iwamoto, T., and Kabuto, C. The First Isolable Dialkylsilylene. *Journal of the American Chemical Society*, 121(41):9722-9723, 1999.

[23] Ishida, S., Iwamoto, T., Kabuto, C., and Kira, M. Insertion of a stable dialkylsilylene into silicon-chlorine bonds. *Silicon Chemistry*, 2(3):137-140, 2003.

[24] Koike, T., Kosai, T., and Iwamoto, T. 1, 4-Dehydrogenation with a Two-Coordinate Cyclic (Alkyl)(amino)silylene. *Chemistry–A European Journal*, 25(39):9295-9302, 2019.

[25] Guha, A. K., and Phukan, A. K. Theoretical Study on the Effect of Annelation and Carbonylation on the Electronic and Ligand Properties of *N*-Heterocyclic Silylenes and Germylenes: Carbene Comparisons begin To Break Down. *The Journal of Organic Chemistry*, 79(9):3830-3837, 2014.

[26] The ylide stabilized CAASis/CAAGes can be represented by two different resonance structures **A** and **B** (shown below for molecule **8** as a representative example). **A** represents a double-bonded form (as shown in Scheme 3.2) while **B** represents a zwitterionic form in which the negative and positive charges are placed at carbon and phosphorus atoms respectively.

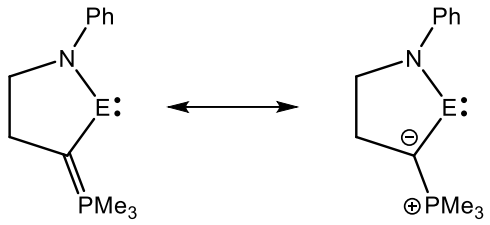

A **B**

E = Si, Ge

[27] (a) Zhao, Y., and Truhlar, D. G. The M06 suite of density functionals for main group thermochemistry, thermochemical kinetics, noncovalent interactions, excited states, and transition elements: two new functionals and systematic testing of four M06-class functionals and 12 other functionals. *Theoretical Chemistry Accounts*, 120(1):215-241, 2008; (b) Walker, M., Harvey, A. J., Sen, A., and Dessent, C. E. Performance of M06, M06-2X, and M06-HF Density Functionals for Conformationally Flexible Anionic Clusters: M06 Functionals Perform Better than B3LYP for a Model System with Dispersion and Ionic Hydrogen-Bonding Interactions. *The Journal of Physical Chemistry A*, 117(47):12590-12600, 2013; (c) Leverentz, H. R., and Truhlar, D. G. Assessment of New Meta and Hybrid Meta Density Functionals for Predicting the Geometry and Binding Energy of a Challenging System: the Dimer of H_2S and Benzene. *The Journal of Physical Chemistry A*, 112(26):6009-6016, 2008; (d) Sethio, D., Raggi, G., Lindh, R., and Erdélyi, M. Halogen Bond of Halonium Ions: Benchmarking DFT Methods for the Description of NMR Chemical Shifts. *Journal of Chemical Theory and Computation*, 16(12):7690-7701, 2020; (e) Valero, R., Costa, R., de PR Moreira, I., Truhlar, D. G., and Illas, F. Performance of the M06 family of exchange-correlation functionals for predicting magnetic coupling in organic and inorganic molecules. *The Journal of Chemical Physics*, 128(11): 114103, 2008; (f) Yang, Y. F., Hong, X., Yu, J. Q., and Houk, K. N. Experimental–Computational Synergy for Selective Pd(II)-Catalyzed C–H Activation of Aryl and Alkyl Groups. *Accounts of Chemical Research*, 50(11):2853-2860, 2017.

[28] (a) Weigend, F., and Ahlrichs, R. Balanced basis sets of split valence, triple zeta valence and quadruple zeta valence quality for H to Rn: Design and assessment of accuracy. *Physical Chemistry Chemical Physics*, 7(18):3297-3305, 2005; (b) Weigend, F. Accurate Coulomb-fitting basis sets for H to Rn. *Physical Chemistry Chemical Physics*, 8(9):1057-1065, 2006.

[29] (a) Reed, A. E., Curtiss, L. A., and Weinhold, F. Intermolecular Interactions from a Natural Bond Orbital, Donor-Acceptor Viewpoint. *Chemical Reviews*, 88(6):899-926, 1988; (b) Glendening, E. D., Reed, A. E., Carpenter,J. E., and Weinhold, F. NBO Program 3.1, W. T. Madison, 1988.

[30] Frisch, M. J., Trucks, G. W., Schlegel, H. B., Scuseria, G. E., Robb, M. A., Cheeseman, J. R., Montgomery, J. A., Jr., Vreven, T., Kudin, K. N., Burant, J. C., Millam, J. M., Iyengar, S. S., Tomasi, J., Barone, V., Mennucci, B., Cossi, M., Scalmani, G., Rega, N., Petersson, G. A., Nakatsuji, H., Hada, M., Ehara, M., Toyota, K., Fukuda, R., Hasegawa, J., Ishida, M., Nakajima, T., Honda, Y., Kitao, O., Nakai, H., Klene, M., Li, X., Knox, J. E., Hratchian, H. P., Cross, J. B., Bakken, V., Adamo, C., Jaramillo, J., Gomperts, R., Stratmann, R. E., Yazyev, O., Austin, A. J., Cammi, R., Pomelli, C., Ochterski, J. W., Ayala, P. Y., Morokuma, K., Voth, G. A., Salvador, P. J., Dannenberg, J., Zakrzewski, V. G., Dapprich, S., Daniels, A. D., Strain, M. C., Farkas, O., Malick, D. K., Rabuck, A. D., Raghavachari, K., Foresman, J. B., Ortiz, J. V., Cui, Q., Baboul, A. G., Clifford, S., Cioslowski, J., Stefanov, B. B., Liu, G., Liashenko, A., Piskorz, P., Komaromi, I., Martin, R. L., Fox, D. J., Keith, T., Al- Laham, M. A., Peng, C. Y., Nanayakkara, A., Challacombe, M., Gill, P. M. W., Johnson, B., Chen, W., Wong, M. W., Gonzalez, C., and Pople, J. A. *Gaussian 03*, *Revision D.02*; Gaussian, Inc., Pittsburgh, PA, 2003.

[31] (a) Cossi, M., Scalmani, G., Rega, N., and Barone, V. New developments in the polarizable continuum model for quantum mechanical and classical calculations on molecules in solution. *The Journal of Chemical Physics*, 117(1):43-54, 2002; (b) Tomasi, J., and Persico, M. Molecular Interactions in Solution: An Overview of Methods Based on Continuous Distributions of the Solvent. *Chemical Reviews*, 94(7):2027-2094, 1994; (c) Tomasi, J., Mennucci, B., and Cammi, R. Quantum Mechanical Continuum Solvation Models. *Chemical Reviews*, 105(8):2999-3094, 2005.

[32] Grimme, S., Antony, J., Ehrlich, S., and Krieg, H. A consistent and accurate ab initio parametrization of density functional dispersion correction (DFT-D) for the 94 elements H-Pu. *The Journal of Chemical Physics*, 132(15):154104, 2010.

[33] (a) Bourissou, D., Guerret, O., Gabbaï, F. P., and Bertrand, G. Stable Carbenes. *Chemical Reviews*, 100(1):39-92, 2000; (b) Gronert, S., Keeffe, J. R., and More O'Ferrall, R. A. Stabilities of Carbenes: Independent Measures for Singlets and Triplets. *Journal of the American Chemical Society*, 133(10):3381-3389, 2011.

[34] (a) Ogata, H., Lubitz, W., and Higuchi, Y. [NiFe] hydrogenases: structural and spectroscopic studies of the reaction mechanism. *Dalton Transactions*, (37):7577-7587, 2009; (b) Dey, S., Das, P. K., and Dey, A. Mononuclear iron hydrogenase. *Coordination Chemistry Reviews*, 257(1):42-63, 2013; (c) Shima, S., and Thauer, R. K. A third type of hydrogenase catalyzing H_2 activation. *The Chemical Record*, 7(1):37-46, 2007.

[35] Vries, J. G. de and Elsevier, C. J. (2007). Handbook of homogeneous hydrogenation, Wiley-VCH, Weinheim.

[36] Tye J. W. and Hall, M. B. (2006). in *Activation of Small Molecules: Organometallic and Bioinorganic Perspectives*. ed. W. B. Tolman, Wiley-VCH, Weinheim, Germany, pages. 121-150; (b) Crabtree, R. H. (2009). *The Organometallic Chemistry of The Transition Metals*. John Wiley & Sons, New York; (c) Kubas, G. J. (2001). *Metal Dihydrogen and σ-Bond Complexes: Structure, Theory, and Reactivity*, Kluwer Academic/Plenum Publishers, New York; (d) Kubas, G. J. Fundamentals of H_2 Binding and Reactivity on Transition Metals Underlying Hydrogenase Function and H_2 Production and Storage. *Chemical Reviews*, 107(10):4152-4205, 2007.

[37] Spikes, G. H., Fettinger, J. C., and Power, P. P. Facile Activation of Dihydrogen by an Unsaturated Heavier Main Group Compound. *Journal of the American Chemical Society*, 127(35):12232-12233, 2005.

[38] (a) Kubas, G. J. Breaking the H_2 Marriage and Reuniting the Couple. *Science*, 314(5802): 1096-1097, 2006; (b) Kenward, A. L., and Piers, W. E. Heterolytic H_2 activation by nonmetals. *Angewandte Chemie International Edition*, 47(1):38-41, 2008; (c) Driess, M. Breaking the limits with silylenes. *Nature Chemistry*, 4(7):525-526, 2012; (d) Power, P. P. Main-group elements as transition metals. *Nature*, 463(7278):171-177, 2010; (e) Erős, G., Mehdi, H., Pápai, I., Rokob, T. A., Király, P., Tárkányi, G., and Soós, T. Expanding the Scope of Metal-Free Catalytic Hydrogenation through Frustrated Lewis Pair Design. *Angewandte Chemie International Edition*, 122(37):6709-6713,

2010; (f) Himmel, H. J., and Vollet, J. Probing the Reactivity of Aluminum(I) Compounds: The Reaction of Pentamethylcyclopentadienyl-aluminum, $Al[C_5(CH_3)_5]$, Monomers with Dihydrogen in a Solid Ar Matrix to Give the New Aluminum Hydride Molecule $H_2Al[C_5(CH_3)_5]$. *Organometallics*, 21(26): 5972-5977, 2002; (g) Peng, Y., Brynda, M., Ellis, B. D., Fettinger, J. C., Rivard, E., and Power, P. P. Addition of H_2 to distannynes under ambient conditions. *Chemical Communications*, (45):6042-6044, 2008; (h) Li, J., Schenk, C., Goedecke, C., Frenking, G., and Jones, C. A Digermyne with a Ge–Ge Single Bond that Activates Dihydrogen in the Solid State. *Journal of the American Chemical Society*, 133(46):18622-18625, 2011; (i) Protchenko, A. V., Birjkumar, K. H., Dange, D., Schwarz, A. D., Vidovic, D., Jones, C., Kaltsoyannis, N., Mountford, P., and Aldridge, S. A Stable Two-Coordinate Acyclic Silylene. *Journal of the American Chemical Society*, 134(15):6500-6503, 2012; (j) Chu, T., and Nikonov, G. I. Oxidative Addition and Reductive Elimination at Main-Group Element Centers. *Chemical Reviews*, 118(7):3608-3680, 2018; (k) Takahashi, S., Bellan, E., Baceiredo, A., Saffon-Merceron, N., Massou, S., Nakata, N., Hashizume, D., Branchadell, V., and Kato, T. A Stable N-Hetero-*Rh*-Metallacyclic Silylene. *Angewandte Chemie International Edition*, 58(30):10310-10314, 2019; (l) Protchenko, A. V., Schwarz, A. D., Blake, M. P., Jones, C., Kaltsoyannis, N., Mountford, P., and Aldridge, S. A Generic One-Pot Route to Acyclic Two-Coordinate Silylenes from Silicon(IV) Precursors: Synthesis and Structural Characterization of a Silylsilylene. *Angewandte Chemie International Edition*, 52(2):568-571, 2013; (m) Wendel, D., Porzelt, A., Herz, F. A., Sarkar, D., Jandl, C., Inoue, S., and Rieger, B. From Si(II) to Si(IV) and Back: Reversible Intramolecular Carbon–Carbon Bond Activation by an Acyclic Iminosilylene. *Journal of the American Chemical Society*, 139(24):8134-8137, 2017; (n) Peng, Y., Guo, J. D., Ellis, B. D., Zhu, Z., Fettinger, J. C., Nagase, S., and Power, P. P. Reaction of Hydrogen or Ammonia with Unsaturated Germanium or Tin Molecules under Ambient Conditions: Oxidative Addition versus Arene Elimination. *Journal of the American Chemical Society*, 131(44):16272-16282, 2009; (o) Usher, M., Protchenko, A. V., Rit, A., Campos, J., Kolychev, E. L., Tirfoin, R., and Aldridge, S. A Systematic Study of Structure and E−H Bond Activation Chemistry by Sterically Encumbered Germylene Complexes. *Chemistry–A European Journal*, 22(33):11685-11698, 2016.

[39] (a) Bharadwaz, P., Chetia, P., and Phukan, A. K. Electronic and Ligand Properties of Skeletally Substituted Cyclic (Alkyl)(Amino) Carbenes (CAACs) and

Their Reactivity Towards Small Molecule Activation: A Theoretical Study. *Chemistry–A European Journal*, 23(41):9926-9936, 2017; (b) Devarajan, D., Doubleday, C. E., and Ess, D. H. Theory of Divalent Main Group H_2 Activation: Electronics and Quasiclassical Trajectories. *Inorganic Chemistry*, 52(15):8820-8833, 2013; (c) Wang, Y., and Ma, J. Silylenes and germylenes: The activation of H–H bond in hydrogen molecule. *Journal of Organometallic Chemistry*, 694(16), 2567-2575, 2009; (d) Nyíri, K., Szilvási, T., and Veszprémi, T. The mechanism and energetics of insertion reactions of silylenes. *Dalton Transactions*, 39(39):9347-9352, 2010.

[40] Alberto, M. E., Russo, N., and Sicilia, E. EH_3 (E= N, P, As) and H_2 Activation with N-Heterocyclic Silylene and Germylene Homologues. *Chemistry–A European Journal*, 19(24):7835-7846, 2013.

[41] Max Appl., (1999). Ammonia: principles and industrial practice, Wiley.

[42] van der Vlugt, J. I. Advances in Selective Activation and Application of Ammonia in Homogeneous Catalysis. *Chemical Society Reviews*, 39(6):2302-2322, 2010.

[43] (a) Hadlington, T. J., Abdalla, J. A., Tirfoin, R., Aldridge, S., and Jones, C. Stabilization of a two-coordinate, acyclic diaminosilylene (ADASi): completion of the series of isolable diaminotetrylenes, $:E(NR_2)_2$ (E= group 14 element). *Chemical Communications*, 52(8):1717-1720, 2016; (b) Jana, A., Objartel, I., Roesky, H. W., and Stalke, D. Cleavage of a N−H Bond of Ammonia at Room Temperature by a Germylene. *Inorganic Chemistry*, 48(3):798-800, 2009; (c) Wang, W., Inoue, S., Yao, S., and Driess, M. Reactivity of N-heterocyclic Germylene Toward Ammonia and Water. *Organometallics*, 30(23):6490-6494, 2011.

[44] (a) Yao, S., van Wüllen, C., Sun, X. Y., and Driess, M. Dichotomic Reactivity of a Stable Silylene toward Terminal Alkynes: Facile C–H Bond Insertion versus Autocatalytic Formation of Silacycloprop-3-ene. *Angewandte Chemie International Edition*, 47(17):3250-3253, 2008; (b) Jana, A., Samuel, P. P., Tavčar, G., Roesky, H. W., and Schulzke, C. Selective Aromatic C−F and C−H Bond Activation with Silylenes of Different Coordinate Silicon. *Journal of the American Chemical Society*, 132(29):10164-10170, 2010; (c) Miller, K. A., Watson, T. W., Bender IV, J. E., Banaszak Holl, M. M., and Kampf, J. W. Intermolecular C−H Insertions and Cyclization Reactions Involving a Stable Germylene. *Journal of the American Chemical Society*, 123(5):982-983, 2001.

[45] (a) Bharadwaz, P., Dewhurst, R. D., and Phukan, A. K. Metal-Free Activation of Enthalpically Strong Bonds: Unraveling the Potential of Hitherto Unexplored Singlet Carbenes. *Advanced Synthesis & Catalysis*, 360(23):4543-4561, 2018; (b) Ghosh, B., and Phukan, A. K. Probing the potential of metalla-N-heterocyclic carbenes towards activation of enthalpically strong bonds. *Dalton Transactions*, 49(27):9505-9515, 2020.